materials

MDPI

Review

A Review on Thermophotovoltaic Cell and Its Applications in Energy Conversion: Issues and Recommendations

Mansur Mohammed Ali Gamel [1], Hui Jing Lee [2], Wan Emilin Suliza Wan Abdul Rashid [3], Pin Jern Ker [1,*], Lau Kuen Yau [4], Mahammad A. Hannan [1] and Md. Zaini Jamaludin [3]

[1] Institute of Sustainable Energy, College of Engineering, Universiti Tenaga Nasional, Kajang 43000, Malaysia; mansur.gamel@uniten.edu.my (M.M.A.G.); Hannan@uniten.edu.my (M.A.H.)
[2] Department of Electrical and Electronics Engineering, College of Engineering, Universiti Tenaga Nasional, Kajang 43000, Malaysia; LHJing@uniten.edu.my
[3] Institute of Power Engineering, College of Engineering, Universiti Tenaga Nasional, Kajang 43000, Malaysia; Emilin@uniten.edu.my (W.E.S.W.A.R.); Mdzaini@uniten.edu.my (M.Z.J.)
[4] State Key Laboratory of Modern Optical Instrumentation, College of Optical Science and Engineering, Zhejiang University, Hangzhou 310027, China; 0621072@zju.edu.cn
* Correspondence: pinjern@uniten.edu.my; Tel.: +60-16-6395329

Abstract: Generally, waste heat is redundantly released into the surrounding by anthropogenic activities without strategized planning. Consequently, urban heat islands and global warming chronically increases over time. Thermophotovoltaic (TPV) systems can be potentially deployed to harvest waste heat and recuperate energy to tackle this global issue with supplementary generation of electrical energy. This paper presents a critical review on two dominant types of semiconductor materials, namely gallium antimonide (GaSb) and indium gallium arsenide (InGaAs), as the potential candidates for TPV cells. The advantages and drawbacks of non-epitaxy and epitaxy growth methods are well-discussed based on different semiconductor materials. In addition, this paper critically examines and summarizes the electrical cell performance of TPV cells made of GaSb, InGaAs and other narrow bandgap semiconductor materials. The cell conversion efficiency improvement in terms of structural design and architectural optimization are also comprehensively analyzed and discussed. Lastly, the practical applications, current issues and challenges of TPV cells are critically reviewed and concluded with recommendations for future research. The highlighted insights of this review will contribute to the increase in effort towards development of future TPV systems with improved cell conversion efficiency.

Keywords: thermophotovoltaic; InGaAs; GaSb; narrow bandgap; performance

Citation: Gamel, M.M.A.; Lee, H.J.; Rashid, W.E.S.W.A.; Ker, P.J.; Yau, L.K.; Hannan, M.A.; Jamaludin, M.Z. A Review on Thermophotovoltaic Cell and Its Applications in Energy Conversion: Issues and Recommendations. *Materials* **2021**, *14*, 4944. https://doi.org/10.3390/ma14174944

Academic Editor: Alexander N. Obraztsov

Received: 9 July 2021
Accepted: 15 August 2021
Published: 30 August 2021

1. Introduction

A TPV system converts thermal radiations from various heat sources such as the combustion of fuels, industrial waste heat, concentrated solar or nuclear energy into electricity. For example, fossil fuels are the main energy source for world-wide energy consumption. However, they are non-renewable resources that will deplete over time due to impulsive mining. Panayiotou et al. [1] has estimated that 370.41 TWh/yr of waste heat is generated from European industries in 2017. This massive amount of waste heat generation has led to a worldwide concern on the global environmental impact and a quest for efficient use of waste heat in the industries. Therefore, there is an urgent need to explore alternatives to improve waste heat recycling and energy conversion efficiency to minimize the reliance on fossil fuels. In this regard, a thermophotovoltaic (TPV) system appears to be a potential candidate to meet these requirements (The meaning of all short names are available in Appendix A). Moreover, the flexibility of converting various heat energy sources such as solar, nuclear, chemical combustion, and waste heat into high electrical power density broadens the TPV application ranging from micro-scale to large-scale TPV

generators [2]. For instance, a worldwide potential of 3.1 GW electricity generation using TPV system in steel industry (>1373 K) was estimated by Fraas et al. [3].

In comparison to a solar photovoltaic system, a TPV system works for a longer operation time at a lower radiator heating temperature [4]. A TPV system consists of four main devices: a generator to provide heat energy from the fuel combustion process, a radiator to translate the heat energy into an emission spectrum, a filter to coordinate the emission spectrum to a TPV cell, and lastly a TPV cell to convert the photon radiation into electrical energy [5]. A comprehensive analysis has been conducted in each component of the TPV system to enhance the overall performance. Particularly, the TPV cell, which converts the photon radiation directly into electricity is the core component that contributes to the overall TPV system performance [6]. Therefore, this review comprehensively studied narrow bandgap TPV cells namely the gallium antimonide (GaSb), indium gallium arsenide (InGaAs) and a few other potential narrow bandgap materials such as germanium (Ge), indium arsenide (InAs), indium gallium arsenide antimonide (InGaAsSb), indium arsenide antimonide phosphide (InAsSbP), and indium gallium arsenide antimonide phosphide (InGaAsSbP) TPV cells. Their respective cell performances, improvements and challenges will be highlighted.

Over the last three decades, research on various parts of the TPV system has received tremendous attention. The advantages of noiselessness, high reliability, mechanical stability without moving parts, and a large power density, make TPV suitable for a vast range of terrestrial and space applications. Recently, numerous review papers have been published. In 2014, Ferraria et al. [7] presented and discussed a critical review of the TPV prototypes. In the next year, Daneshvar et al. [8] reviewed the development of all main components, discussed the fundamental and technical challenges facing commercial adoption of TPV and prospects of TPV. Mustafa et al. [9] summarized the progress of combustion-driven thermoelectric (TE) and TPV power generation systems for the years 2000–2016. Datas and Martí [10] reviewed the state of the art and historical development of TPV for space application along with the main competing technologies. Tain et al. [11] reported the recent progress of near-field and far-field radiative heat transfer, various design structures of metamaterials and their properties, and focused on the exploration of tunable radiative wavelength selectivity of nano-metamaterials. More recently, in 2019, Sakakibara et al. [12] reviewed the state of the art of radiator and presented a systematic approach for assessing radiators. A recent paper from Rashid et al. [13] has highlighted the recent development of TPV for waste heat harvesting application and investigated the potential implementation in coal-fired thermal power plant. Furthermore, Burger et al. [14] studied numerous decades of experimental TPV works and compared the energy-conversion of different systems with respect to experiment-specific thermodynamic limit. Based on the research gap, a review on the comparison of performance parameters of different TPV cell materials and their respective improvement and potential are yet to be conducted. Therefore, this paper focuses on the TPV cell, which is the main component in the TPV system. Furthermore, the comprehensive review on various TPV cells contributes to the understanding of the decades of advancement, future prospects, and applications of TPV cells.

The structure of the paper is as follows. Section 2 presents the overall TPV system and the analytical aspects involving the TPV cell conversion. Section 3 summarizes the methods to fabricate TPV cells. Sections 4–6 review GaSb, InGaAs, and other narrow bandgap TPV cells, respectively. The engineering applications are discussed and presented in Section 7. In Section 8, we provide some current challenges and recommendations for future research prospects in this field. Even though not all the issues and challenges in TPV systems can be immediately addressed, recommendations are provided on the current issues which can be potentially resolved. This review will provide a clear and accessible guidance on a complete TPV system and a thorough literature study of TPV cells together with the development, performance, improvement, and the current issues with concrete recommendations.

2. TPV System Overview

A TPV system converts radiant energy from a generator into electrical energy using TPV cells. Figure 1 shows the TPV system which includes a generator, a radiator, a filter and an array of TPV cells [7]. The generator produces power from various heating sources (P_{source}) to the radiator with certain heat loss ($P_{source,loss}$). Next, the radiator generates the radiant power ($P_{radiant}$) to the PV cells via the filter. The filter then narrows the emission band from the radiator. The filtered radiated energy from the radiator should exceed the bandgap of PV cells with the bandgap power (P_{gap}), whereas losses ($P_{gap,loss}$) are induced by the photons with lower energy than the bandgap of PV cells. These photons are recuperated to the radiator ($P_{recuperate}$) to conserve heat and reduce P_{source} at the required radiator temperature. The output power (P_{out}) at PV cells is measured through the optical-to-electrical signal conversion process [7].

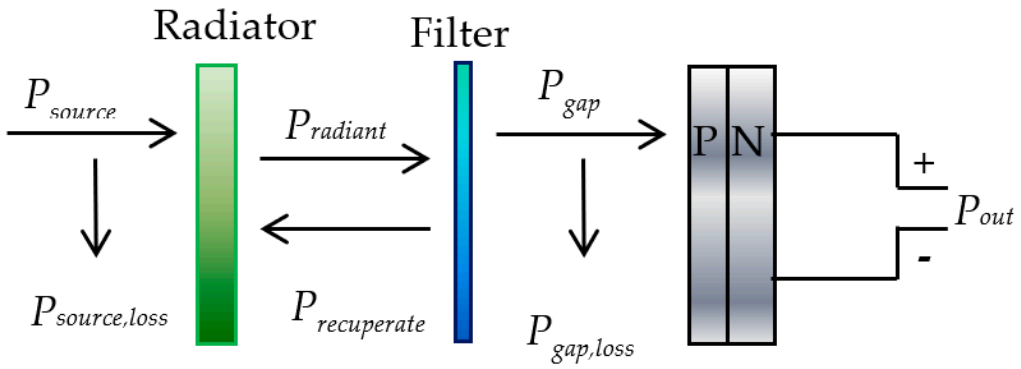

Figure 1. Schematic diagram of an overall TPV system.

A generator is a heat-driven source for TPV system with a typical working temperature range from 1000 to 2000 K [9,15]. This generator can be concentrated solar radiation, radioisotope thermal generator, combustion of hydrocarbon fuels or industrial waste heat [16,17]. Solar radiation produces the highest temperature among the generators. Nevertheless, this high temperature is attained only at the AM 0 condition. Subsequently, the installation angle of TPV cell to harvest solar radiation at AM 1.5 condition should be optimized to achieve higher radiation energy efficiency. Apart from solar radiation and radioisotope, liquid and gas fuels such as oil, butane, propane, methane, and hydrogen are employed to drive a generator [18–25]. Various TPV combustor–regenerator systems for electric vehicles have been studied both theoretically and experimentally [26]. The combustion system was optimized via studying the thermo-fluid dynamic model. Chamber geometry, fuel injection, and mass flow rate were found to be dominant parameters. Furthermore, the heat exchanger optimization was obtained by substituting the matrix material with a ceramic material that is lighter than metal and with a greater heat capacity to store a high amount of energy. Additionally, ceramic matrix was able to obtain a greater porosity and thus a greater surface for the heat exchange with a reduction of volume and weight. Colangelo et al. [27] designed and tested various TPV combustors and heat recovery systems for different testing conditions. It was found that a rotary heat exchanger is an optimal design since it is very compact and has higher effectiveness in comparison with other types of regenerators with the same number of transfer units. Furthermore, the study developed a model which accurately predicts the performance of the heat exchanger, taking into account two different values for the physical properties (such as thermal conductivity, heat capacity) for the hot and cold sides of the regenerator.

A radiator emits electromagnetic energy by translating heat from generators into an emission spectrum to provide appropriate receiver cell sensitivity [22]. Selective radiators such as silicon carbide (SiC), tungsten (W), W-SiO_2 rare-earth oxide, and photonics crystal (PhC) provide narrow spectral range emission by enhancing in-band radiation and suppressing out-of-band radiation [28–34]. There are two significant types of selective radiators,

namely the rare-earth oxide radiator and the broadband radiator [35]. Bitnar et al. [20] reported that the maximum emissivity of ytterbia and erbia radiators is 0.85 at a photon energy of 1.27 eV and 0.82 at a photon energy of 0.80 eV, for temperatures 1735 K and 1680 K, respectively. The bandgap of the selective radiator must be higher than the bandgap of TPV cell to minimize the build-up of recombination for higher electrical energy conversion efficiency purpose. Therefore, Si (1.1 eV) cell is suitable for the ytterbia radiator while GaSb (0.7 eV) TPV cell is suitable for the erbia radiator. A promising radiator has been achieved by vacuum plasma spray coating of rare earth oxides on intermetallic alloy $MoSi_2$. The radiator can operate in an oxygen-containing atmosphere at a temperature of 1873 K, which is highly thermal-shock stable and shows good selective-emitting properties [36].

Broadband radiator establishes the emission across a wide range of wavelength for temperature range between 1000 to 2000 K [32,37]. Examples of broadband radiators are alumina, zirconia, magnesia, silica, yttria, and more, which possess a major challenge in low thermal shock resistance and low emissivity [38]. SiC with a minimum bandgap of 2 eV [39] has proven to be a suitable TPV radiator which can endure high melting point and high emissivity close to a 0.9 μm wavelength at an operating temperature up to 1923 K [38,40]. A SiC porous superadiabatic radiant burner (radiator) was experimentally proposed for TPV system, achieving radiator efficiency up to 32% and a system output power of 5–10 W [41]. A broadband radiator shows advantages over a selective radiator due to the simplicity in fabrication, higher durability and less labor-intensive [35]. Nevertheless, these advantages are attained at the cost of lower TPV system efficiency and power density as compared to selective radiator [23]. Gentillon et al. [42,43] experimentally characterized and analyzed a design of a porous media combustion-based thermophotovoltaic reactor with controlled radiant emission using yttria-stabilized zirconia/alumina composite (YZA). It was found that the erbia coating on YZA foam increases the emissivity by ~10%.

A filter is located in between the radiator and the TPV cell to spectrally filter the emission from the radiator, it is matched to the bandgap of TPV cell to block the energy of photons that is lower than the energy bandgap of a TPV cell [7]. The TPV cell performance is optimized by selectively filtering the thermal radiation depending on the radiator temperature and bandgap of TPV cell. This is to promote photon recycling and to improve system conversion efficiency [20,44]. Catchpole et al. [45] demonstrated that 99% of photon energy sit above the TPV bandgap using a highly idealized filter with 0.7 V applied voltage. Tong et al. [46] proposed on the utilization of intermediate frequency filter and photon recycling back to the radiator. Interference filter or dielectric filter is realized as a multilayer stack which can be deposited over the cell or to be placed between the radiator and the cell. The interface creates a low pass filter that cuts at a specific wavelength [8,47].

TPV cell converts the photon radiation into electricity and share similar principal as PV cell. The total current density flow through the load, J in Figure 2 is expressed as [4]:

$$J = J_o \left(e^{\frac{e_0 V}{kT_{cell}}} - 1 \right) - J_{ph} \quad (1)$$

In the dark condition, there will be no current generated by per unit area, thus the J_{ph} is equal to zero. The relationship between the current and voltage is expressed using Shockley diode equation, as shown in Equation (1). Figure 2 shows the current-voltage (IV) characteristics of the dark cell when the J_{ph} is zero. When the cell is illuminated, each photon above the bandgap (hV_g) will contribute to one elementary charge (e_o), generating the J_{ph}. The IV curve will therefore be shifted to quadrant IV where information about maximum current density (J_m), V_m and maximum power can be extracted. The maximum power output is utilized by the external load, R_L.

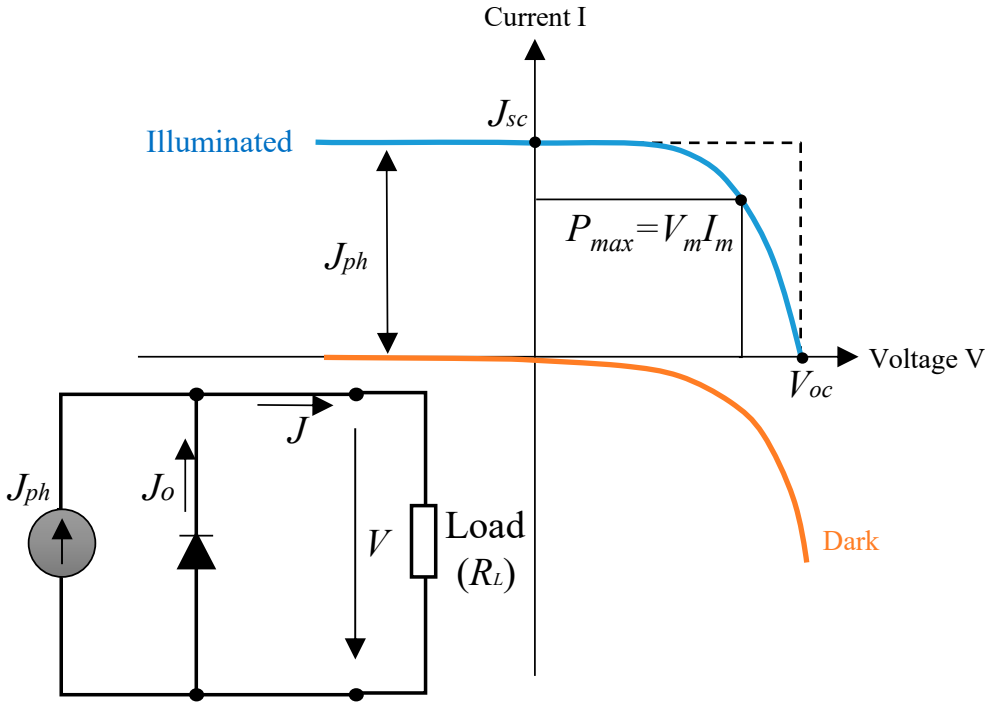

Figure 2. The equivalent circuit and IV characteristics of dark cell when J_{ph} = 0.

All radiated photons must be fully absorbed and converted into photocurrent to achieve a maximum J_{ph}. In this context, the external quantum efficiency (*EQE*) defines the photon-to-photocurrent conversion efficiency of a TPV cell. *EQE(λ)* as a function of λ describes the probability of a photon with wavelength λ absorbed by the cell which generates electron-hole pair that will be collected at the terminal. *EQE(λ)* represents the functionality of p-n junction in detail as it considers both the reflection and absorption coefficient of the incident photon as well as the collection of the minority carriers. *EQE* can be solved from J_{sc}, which is expressed as a function of incident photon flux $\Phi(\lambda)$ given by:

$$J_{sc} = e \int_0^{\lambda_{GAP}} \Phi(\lambda) \cdot EQE\ (\lambda) \cdot d(\lambda) \tag{2}$$

where $d(\lambda)$ is the penetration distance [7]. TPV radiator with temperatures range from 1473 to 2073 K has a low photon emission at 1000 nm wavelength. For emitted photons with energy lower than the bandgap where absorption is not optimum, a selective filter can be used to redirect source and hence improve the efficiency.

The efficiency of TPV system, η_{TPV} to convert radiated heat to electrical power is expressed as follow [48]:

$$\eta_{TPV} = \eta_{sp}\eta = \frac{P_{out}}{P_{radiant}} \tag{3}$$

where η_{sp} is the spectral efficiency of the radiator which is presented as:

$$\eta_{sp} = \frac{\int_0^{\lambda_c} E(\lambda) \cdot \varepsilon\ (\lambda) \cdot \mathrm{d}\lambda}{\int_0 E(\lambda) \cdot \varepsilon\ (\lambda) \cdot \mathrm{d}\lambda} \tag{4}$$

where $E(\lambda)$ is the blackbody spectrum and $\varepsilon(\lambda)$ is the spectral emissivity of the proposed selective radiator metamaterial.

In this regard, it is observed that there are two main scopes which require further study and investigation. Firstly, it is crucial to improve the heat transfer between the heat source and the TPV cell. This can be done by increasing the emissivity and the use of

suitable type of selective radiator. The second approach is to improve the *EQE* of the cell, which leads to higher cell efficiency.

3. TPV Cell Fabrication

There are two methods of TPV cell fabrication, namely non-epitaxial and epitaxial methods. Non-epitaxial growth can be sub-categorized into two: diffusion method and ion implantation method. Diffusion method is commonly used to fabricate GaSb TPV cell [49–51] and InGaAs [52]. The conventional diffused GaSb-based TPV cell is manufactured in a pseudo-closed box (PCB) with the diffusion of Zn particle into Tellurium-doped single-crystal GaSb substrate [53]. Parameters studied on the diffusion profiles are temperature, diffusion time and precision of control for the depth of p-n junction. Tang et al. [49,50] presented a closed-quartz-tube for the diffusion process where Zn-Ga alloy is proven to be a suitable source that can suppress the formation of high concentration surface region in Zn profile with a lower fabrication cost.

Ion implantation method is the most suitable method to perform selective doping, as the spatial distribution of dopant atoms can be more precisely defined [54]. However, the use of ion implantation introduces undesirable damage to the lattice crystal structure due to the high annealing temperature [54–56]. The formation of junctions appears to be more difficult than diffused junctions [57,58]. This causes a non-uniform p-n junction formation due to different thicknesses of the active region. Rahimi et al. [59] demonstrated that the Be-implanted GaSb exhibits similar performance to the MBE-grown GaSb TPV cell. To achieve this, the implanted dopants on the semiconductor substrate must undergo a rapid thermal annealing (RTA) process where the cell is exposed to a high temperature to remove the implant-induced damage and therefore achieving a higher shunt resistance [55,60]. It is highlighted that inadequate isolation is produced from the ion bombardment process due to small intrinsic resistivity of InGaAs material [61]. The main limitation of the non-epitaxial growth method is the high front and back surface recombination which reduce the photocurrent collection. Several studies proposed an advance growth method that combined epitaxial and diffusion method [62,63]. The main advantage of the combined growth technique is to create a device with low surface recombination and low defect density.

Epitaxy is a process of depositing crystalline on a substrate that acts as a seed crystal, which is favorable for achieving a better cell performance with the advantages of better purity control, thickness control and doping level control. The epitaxy can be categorized into three different mediums: liquid, solid and vapor. Liquid phase epitaxy (LPE) is the deposition of liquid phase single-crystalline either in the solution or melt form on a substrate crystal below the melting temperature of deposited materials [64]. Most TPV cell structures are initially fabricated using LPE method due to the simplicity of the process. TPV cells grown by LPE method suffer from very high lattice mismatch [65] and poor thickness control, which affect the cell efficiency. Epitaxial lateral overgrowth (ELOG) is introduced to solve the mismatching issue in heteroepitaxy [66,67]. It is worth highlighting that ELOG blocks mismatching threats from substrate [68]. Cheetham et al. [69] described a well-established low bandgap structure using LPE growth method with $InAs_{0.62}Sb_{0.14}P_{0.24}/Ga_{0.03}In_{0.97}As_{0.83}Sb_{0.14}P_{0.03}$ on InAs substrate. In 2015, Krier et al. [65] developed a $InAs_{0.61}Sb_{0.31}P_{0.26/}$InAs p-n junction with 0.32 eV bandgap using the LPE method. Hence, LPE is a promising technique to produce a larger size single crystal with high-quality binary, ternary and quaternary TPV structures at relatively low growth temperature [70]. Despite the simplicity and low cost of LPE method, vapor phase epitaxy (VPE) is capable of producing cells with better crystal quality and higher performance.

VPE can be subcategorized into molecular beam epitaxy (MBE), metal-organic vapor phase epitaxy (MOVPE) and plasma-enhanced chemical vapor deposition (PECVD). MOVPE method was introduced for the growth of vapor phase III-V compound semiconductor materials, such as GaSb or InSb, on different types of substrate surfaces [71]. MOVPE is suitable for numerous commercialized low bandgap devices, with the advantages of a low reactor downtime, ease of maintenance, easy scalability for multi-wafer

deposition, as well as more stable and controllable growth rates. In addition, MOVPE is more suitable for the growth of high-quality InP buffer and cladding layers due to lower arsenic contamination [72]. MOVPE is often use in high-quality materials and more complex structures with higher interface quality [73]. Material quality can be significantly improved by all parameters which reduce atomic surface diffusivity, such as decreasing growth temperature, increasing growth rate, and substrate miscut angle [74]. TPV cell technology is approaching 30% cell efficiency at 300 K cell temperature due to the gradual improvement in the MOVPE manufacturing process [75]. The experimental data of a simple Zn-diffused GaSb structure as compared to the complex MOVPE structure has proven that MOVPE structure had better performance with a maximum *FF* of 75% as compared to 70% with Zn diffusion structure [76]. One of the essential advantages of MOVPE method is the wide selection range of substrate materials. Most work in the MOVPE-fabricated TPV cells was conducted to improve the density of mismatching using cheaper substrate materials. For an InGaAsSb TPV cell, GaAs substrate is a better option compared to GaSb as the cost is cheaper with a higher potential to be commercialized [77]. Despite high lattice dislocation (7%) between GaSb p-n junction and GaAs substrate, the structure was improved by shifting the active junction away from the substrate material using selective epitaxy technique to create a buffer layer. The output power of GaSb/GaAs cell is only 30% lower than homojunction GaSb cell, under the same illumination condition. In another study, InGaAsSb on GaAs exhibited similar dark current-voltage characteristic with that on GaSb substrate. Furthermore, the J_{SC} and V_{OC} of fabricated structure are comparable with GaSb-based structure under illumination from 1073 K silicon nitride radiator [78]. In another study, Lu et al. [79] reported the use of a novel metamorphic buffer layer to suppress the threading dislocations originating from the large lattice-mismatch of InGaAsSb on GaAs substrate, which included the interfacial misfit arrays at the GaSb/GaAs interface and strained InGaSb/GaSb multi-quantum wells acting as dislocation filtering layers.

MBE utilizes an ultra-high vacuum (UHV) with a low deposition pressure in the chamber (lower than 10 Torr). This technique provides a clean growth environment, higher purity, precise control of the beam fluxes and growth condition by changing the nature of the incoming beam. The MBE method has the advantage of generating complicated doping profiles due to the flexible control of the dopants. The MBE method provides promising fundamental device parameters such as low ideality factor (n = 1.0) and low dark current of 6×10^{-5} A. However, a GaSb structure grown over a large area is challenging due to the difficulty of finding an epi-ready substrate, non-uniform native oxide desorption, and shunt defect formation. A key advantage of using the MBE method to grow TPV cell is the generation of a higher V_{oc} when compared to the MOVPE and LPE methods [59,80]. Table 1 provides a summary of characteristics, advantages and disadvantages for different types of TPV cell growth methods.

Table 1. Characteristics of Different Growth Methods for TPV Cells.

Growth Method		Growth Rate	Heterojunction	Temperature	Vacuum (Y/N)	Safety	Cost	Absorb Thickness	Thickness Control (Y/N)	Absorb Doping	Doping Control (Y/N)
Epitaxial	MBE	0.082–0.278 nm/s [81–83]	Produces super lattice heterostructure structure [84,85]	723–808 K [80,86,87]	An ultra-high vacuum pressure lower than 5×10^{-11} Torr [84,88]	Toxic and required safety system for hydride gases [88]	Very expensive and complex [89]	2–10 µm [80,90–92]	Precise control [60,93]	$8x10^{16}$–$2x10^{17}$ [62,80,91,92,94]	Precise control over doping level and composition [60,93]
	MOVPE	0.0006–0.63 µm/s [93,95–99]	Suitable for heretojunction structure [93,96]	773–903 K [73,93,95–100]	Pressure ranging between 40–600 Torr [97–99,101]	Highly toxic	Expensive equipment and complex than LPE [89]	1–6 µm [96,97,102–105]	Precise control [93,100]	2.2×10^{16}–5×10^{17} [96,97,102–105]	Doping and composition level are highly precise [93,100]
	LPE	2–15 µm/s 10 to 100 times faster than MOVPE or MBE [95,106,107]	Not very suitable	623–883 K [65,67,69,106,108,109]	Slightly above atmosphere pressure [65,69]	Produce non-toxic or less dangerous substances [108,109]	Simple and inexpensive method [108]	2–200 µm [69,107,109]	Less precise [84,95] but it can be improve with lower growth rate [110]	1×10^{17}–5×10^{18} [70,109,111]	n/a
Non-Epitaxial	Diffusion	2–5 h to complete the diffusion [49,112]	Not suitable	693–753 K [62,113,114]	Diffusion closed box at vacuum level [49]	n/a	Simple and inexpensive	100–400 µm	n/a	3×10^{17}–2.3×10^{20} [52,62,111]	Less precise [113]
	Ion implantation	n/a	Not suitable	80–373 K [115]	300–1000 Torr [116]	Ionized radiation	Less expensive [60]	100–400 µm	n/a	n/a	Precise control

4. GaSb-Based TPV Cell

In this section, a comprehensive study on GaSb-based TPV cell in terms of their historical development, cell performance, performance improvements and challenges are thoroughly discussed.

4.1. Introduction

GaSb is a III-V binary semiconductor compound. It is considered as one of the ideal semiconductor materials for TPV applications with temperature source ranging from 1300 K to 1500 K. Due to its low bandgap energy (E_g), which spectrally matched with the medium blackbody temperature, it produces an excellent quantum efficiency of greater than 90%, especially at IR wavelength up to 1800 nm [117]. A few advantages of the GaSb semiconductor material compared to the other conventional materials such as Si, Ge are the direct bandgap properties with 0.72 eV energy at 300 K, and the cell performance is less affected at higher operating temperature [118]. Historically, in 1989, Dr. Lewis Fraas invented a GaSb photocell using Zn diffusion method as a booster cell, mechanically stacked under GaAs material for concentrator solar cell application [119], with a world-record energy conversion efficiency of 35% [53,120]. Later in 1995, there is a major breakthrough of an electric generator using GaSb TPV cells with a hydrocarbon burner patented by Fraas and associates [121]. In addition, JX Crystal Inc. commercialized the "Midnight Sun" TPV stove for residential heating application in 1995 [21]. Morrison and Seal successfully built a prototype of the world's first TPV-powered automobile named "Viking 29" which utilizes 20 series connected GaSb cells with over 41 W power generation [122,123]. In the 2000s, Stollwerk et al. [124] conducted the first simulation on GaSb TPV cell using two-dimensional (2-D) numerical solar cell simulation program. The advancement in material widens the opportunity for the researchers to explore various TPV applications.

Nowadays, the GaSb TPV cells are technologically matured and commercially available. Research efforts towards maximizing the conversion efficiency increase tremendously in the recent years. In 2014, GaSb TPV cell is used to generate electricity from waste heat in the steel industry which generates 3.1 GW of power under 1673 K [3]. Recently, an evaluation study of GaSb TPV cell performance at low-, mid- and high-waste heat temperature was conducted by researchers in Turkey targeting the potential waste heat location in the Turkish Industrial Sector [125–127]. The GaSb-based TPV cell is currently an active research area and expected to be continually developed in the near future. Taking advantage of its infrared radiation sensitivity, the GaSb TPV cell has great potential for waste heat energy harvesting. Significantly, the research on GaSb for TPV applications is advancing rapidly since the industrial processing and activities have been constantly emitting a huge amount of potential waste heat to be recovered.

4.2. Performance of GaSb-Based TPV Cell

The early GaSb photovoltaic cell structure that is sensitive to the photons in the infrared region up to 1.8 μm was invented and patented in 1988 by McLeod et al. (see US 4,776,893 [128] patent) and Fraas et al. (see US 5096505 [129] and US 5091,018 [130] patent). The cell was intentionally designed to be used as an infrared booster cell stacked tandemly under GaAs solar cell for concentrated sunlight solar application. Since the early invention, the performance of a single GaSb cell under 100 suns concentrated light intensities was recorded with an FF of 71.3%, V_{oc} of 0.48 V, and J_{sc} of 2702 mA/cm^2 [130]. Additionally, around a 7% conversion efficiency of GaSb solar cell under the full sunlight spectrum range was recorded through the fundamental characterization studies [53]. Therefore, GaSb cell provides a good electrical performance for infrared radiation capture.

As aforementioned, a major breakthrough in GaSb TPV cell development was made in 1995 by JX Crystal Inc (Fraas and associates). Fraas et al. [131] has developed a prototype of a combined home furnace-TPV generator and reported a much higher power output. Under a SiC blackbody radiator at 1523 K, over 1 W/cm^2 of power output density per

cell was demonstrated. Later on in 2014, Fraas et al. [3] projected a TPV planar module performance for steel industry application at 1400 K and 1500 K blackbody temperature with 20% efficiency and output power of 1.8 W/cm^2. Subsequently, a cell efficiency of 29% with an electric power of 1.5 W/cm^2 for a single GaSb cell measured under 1548 K radiator temperature was reported. Several studies benchmarked their GaSb TPV cells performance with a fabricated device by JX Crystals Inc. For example, Tang et al. [49] demonstrated a new Zn diffusion process for GaSb-based TPV cells. The cell demonstrated a lower performance as compared to JX Crystals Inc device due to the higher series resistance at both front and back electrodes. In contrast, Ni et al. [117] compared an epitaxially grown, thin-film GaSb TPV cell and reported higher theoretical *IQE* performance in comparison to the device fabricated by Fraas et al. [94]. It is highlighted that the epitaxial GaSb TPV can reach approximately 96% of *IQE* when optimizing the emitter and base layer thickness to 0.22 and 10 µm, respectively. In the same vein, Rashid et al. [5] investigated the effect of emitter layer region and compared the GaSb TPV cell performance with a Zn-diffused commercialized JX Crystals Inc device. Based on their simulation result, an efficiency increment from 4.70 to 7.88% was recorded with optimized emitter thickness and doping concentration under AM 1.5 illumination condition.

Several studies have made comparisons between epitaxially grown and non-epitaxially grown (ion-implantation and diffusion) GaSb TPV cells. For example, Martin et al. [132] and Rahimi et al. [59] compared the performance of epitaxial and non-epitaxial GaSb TPV cells. Rahimi emphasized that an annealing process removed implant-induced damage crystal on GaSb devices, resulting in comparable device quality with epitaxially grown GaSb TPV cell. The performance of both epitaxial and non-epitaxial GaSb TPV cells are comparable and suitable to be employed for TPV generators. This statement was supported by Schlegl et al. [76] who demonstrated a slightly better performance of the MOVPE-grown GaSb TPV cell when compared to the Zn-diffused cell. Nevertheless, the method for the epitaxially grown device is more sophisticated and expensive. To date, the GaSb cell fabricated by Zn diffusion method is favorable in various TPV applications due to the simplicity of the fabrication technique. The performance of various single GaSb cells fabricated by Zn diffusion method are summarized in Table 2. However, previous experiments involved various radiation temperature and sources, thus, the highest efficiency is difficult to be concluded for the Zn-diffused GaSb TPV cell technology. Recently, research efforts focus on optimizing the GaSb TPV cell structure to improve the cell performance. For example, the incorporation of wide bandgap window layers and optimization works on the cell configuration have been widely investigated.

In terms of GaSb TPV cells implementation, Khvostikov et al. [133] compared the performance of Zn-diffused GaSb-based TPV arrays connected in both series and parallel configuration. The parallel connection in the cylindrical system was found to produce a better performance when compared to the series connection in a conical system. A photocurrent of 3.58 A was recorded for cylindrical GaSb-based TPV arrays. Consecutively, Khvostikov further measured the performance of a cylindrical TPV system under tungsten (W) and silicon carbide (SiC) radiators [134]. A cell performance of V_{oc} = 0.48, J_{sc} = 4.5 mA/cm^2 and FF = 65% was reported under a 1900 K SiC radiator temperature. Furthermore, a cell efficiency of 19% was recorded using a W radiator. The configuration of photoconverters in the TPV system was well-studied, where higher power output can be produced with higher number of photoconverters. On the other hand, Wu et al. [135] performed an experimental analysis on a TPV system with a SiC radiator to compare the output power density of a single GaSb and Si cell under the same operating condition. It was reported that the GaSb cell produces up to 11 times higher power density when compared to a single Si cell. An output power density of 0.26 W/cm^2 was realized for a single GaSb-based TPV cell under an operating SiC radiator of 1223 K temperature.

Table 2. The performance comparison of Zn-diffused GaSb TPV cell.

Ref	Highlighted Condition	T_{rad} (K)	T_{cell} (K)	V_{oc} (V)	I_{sc} (A)	J_{sc} (mA/cm^2)	FF (%)	P_{max} (W/cm^2)	η_{cell} (%)	Exp./ Pred.
[131]	Consists of shingle mounted 72 GaSb cells	1523	323	11.94	18.76	n/a	68.0	1.0	n/a	Exp.
	Performance assumed at cell temperature at 323 K	1533	323	n/a	n/a	n/a	n/a	n/a	15.4	Pred.
[133]	Consists of GaSb cells array connected in series in a conical TPV system	1673	n/a	1.77	1.05	n/a	66.4	n/a	n/a	Exp.
	Consists of GaSb cells array connected in parallel in a cylindrical TPV system	1673	n/a	0.41	3.5	n/a	62.4	n/a	n/a	
	Zn diffusion source using a polymer film layer	AM 1.5	n/a	0.5	n/a	38.56	66	n/a	n/a	
[134]	Consists of GaSb arrays of 4×3 cells	AM 1.5	n/a	1.69	3.55	n/a	64.1	3.8	4.5	Exp.
	Operated under W radiator	1900	n/a	~0.48	n/a	n/a	~70	n/a	19	
	Operated under SiC radiator		n/a	0.48	n/a	4.5	65	n/a	n/a	
[135]	SiC radiator with 1.1 cm radiator-cell distance	1223	325.2	0.34	2.29	n/a	n/a	0.26	n/a	Exp.
[49]	A silver metal was used to reduce fabrication cost	AM 1.5	n/a	0.281	n/a	29.0	48.5	n/a	3.9	Exp.
	Characterization on the JXC's commercialised cell	AM 1.5	n/a	0.326	n/a	32.3	52.7	n/a	5.5	
[3]	Consists of 10×14 GaSb TPV cells circuit	1773	n/a	n/a	n/a	n/a	n/a	1.8	20	Pred.
		1573	n/a	n/a	n/a	n/a	n/a	1.1	18	Pred.
	Single cell measurement	1548	n/a	n/a	n/a	n/a	n/a	1.5	29	Exp.

Note: n/a means no data available in the literature. T_{rad} is the radiation temperature under measure. Exp. stands for experimental data and Pred. means simulation or mathematical model. Collaboration work of JX Crystal Inc. and a research group in Hohai University, Nanjing, China published several papers on the enhancement of GaSb TPV cells [50,51,136]. In 2015, they reported that the performance of GaSb TPV cell can be improved using n-type emitters at the front-side of the TPV cell active area with PC1D software simulation [51]. In addition, a recent optimized design of a heterojunction on p-doped GaSb with hydrogenated amorphous Si interface passivation has been presented with the *IQE* surpasses 90% and power output density of 2 W/cm^2 in the short-wave range under a blackbody radiation of 1500 K [136]. In principle, TPV cells operate at their optimum performance when GaSb energy bandgap is spectrally matched to the blackbody spectrum [4]. Therefore, the choice of utilizing the GaSb TPV cells is highly dependent on the source of radiation temperature or the types of radiators used in the system.

4.3. Performance Improvements

Research efforts towards maximizing the conversion efficiency have been drastically increased in recent years. Improvements in terms of spectral control [137], metal contact [138–142] as well as optimization on the layer thickness [51,92,117] and doping concentrations [50,51,143,144] are the major topics reported from various works.

4.3.1. Metal Contact Optimization

A metal contact is required to generate electricity by providing a connection between the active semiconductor devices and the external circuit [139]. Good metal contact with low electrical resistance, often referred to as an ohmic contact, is essential to minimize the loss of electrical power and maximize the overall efficiency. The properties of an ohmic contact include good thermal stability, low resistance and good adhesion on the semiconductor surface [139]. Milnes and Polyakov [145] discussed that formation of an ohmic contact on p-type GaSb may involve Au or AuZn for doping concentration of 6×10^{-17} cm^{-3}. Consecutively, Milnes et al. [146] studied and compared Au, Ag and In for p-GaSb with doping concentration between 8×10^{16} cm^{-3} and 1×10^{19} cm^{-3}. It was found that the contact resistivity is inversely proportional to the doping concentration. At doping concentration of 10^{18} cm^{-3}, the contact resistance exhibited values around 5×10^{-5} Ωcm^2. From their finding, it was demonstrated that lower contact resistances are favorable to form ohmic contact on p-GaSb.

On the other hand, materials such as nickel (Ni) and palladium (Pd) metals are found to be suitable candidates to form an ohmic contact on n-GaSb. In contrast to Pd metal, the intermetallic formation of Ni can be performed at a lower temperature. Rahimi et al. [139] reported that Ni metal can easily form a contact on n-GaSb and produces lower resistance and better ohmic characterization than a Pd metal. Other than that, Ge,

gold (Au), platinum (Pt) and molybdenum (Mo) metals are often deposited to form a metallization scheme that produces good ohmic contact on the n-GaSb semiconductor. Each metal shows the advantage of low contact resistance towards the semiconductor. In particular, Rahimi et al. [141] reported a remarkable reduction in contact resistance by optimizing the annealing temperature windows of different metallization schemes for n-GaSb//(Pd+Mo)/Ge/Au/Pt/Au and n-GaSb//Ge/Au/(Pd+Mo)/Pt/Au metallization.

It is worth noting that metal contact is influenced by the doping concentration of semiconductor. Therefore, the difficulty to remove the oxide layer from a highly doped n-type GaSb material prior to the contact metallization is a disadvantage in the formation of ohmic contact. The fabrication and metallization techniques should be further developed to facilitate the formation of a good ohmic contact on n-GaSb, which supports the high photogeneration in TPV cell. Table 3 summarizes the reported metallization, specific contact resistance and metal-forming process on GaSb semiconductor layers.

Table 3. The reported metal contact optimization work.

Ref	GaSb Layer Type	Doping Concentration	Metallization	Specific Contact Resistance	Metal Forming Process
[145]	p-type	8×10^{17} cm^{-3}	Au	1×10^{-4} Ω cm^2	Annealing process with T = 523–623 K
			AuZn	1×10^{-5} Ω cm^2	
	n-type	n/a	Au, AuTe, AuSn	0.5–1 $\times 10^{-4}$ Ω cm^2	Annealing process with T = 523 K
[146]	p-type	8×10^{16} cm^{-3}–1×10^{19} cm^{-3}	Au, Au(Zn), Au(In, Zn), Au(Ge), Ag(Sn), Ag(In), In, In(Zn), In(Ge) and Al	~5×10^{-5} Ω cm^2 for doping 10^{18} cm^{-3} ~5×10^{-6} Ω cm^2 for doping 1×10^{19} cm^{-3}	Annealing process with T = 523–623 K for 10–30 min
[147]	n-type	1.2×10^{18} cm^{-3}	Pd/Ge/Au/Pt/Au	1×10^{-5} Ω cm^2	RTA at T = 543 K for 60 s
[141]	n-type	5×10^{18} cm^{-3}–1×10^{19} cm^{-3}	(Pd+Mo)/Ge/Au/Pt/Au	3×10^{-6} Ω cm^2	RTA at T = 573 K for 45 s
			Ge/Au/(Pd+Mo)/Pt/Au	2×10^{-4} Ω cm^2	RTA at T = 553 K for 45 s
[138]	n-type	5×10^{17} cm^{-3}–1×10^{19} cm^{-3}	Ni/Ge/Au/Pt/Au, Pd/Ge/Au/Pt/Au, Ge/Au/Ni/Pt/Au, Ge/Au/Pd/Pt/Au	1×10^{-2} Ω cm^2–1×10^{-6} Ω cm^2	RTA at T = 533–593 K for 45 s

4.3.2. Thickness, Doping and Design Structure Optimization

The GaSb TPV cell performance parameters exhibit a strong dependence on the layer thickness, doping concentration and junction configuration. Therefore, researchers optimize these parameters to achieve maximum performance efficiency. An optimization of Zn-diffused GaSb emitter can improve the cell performance due to the formation of stronger built-in field that leads to a better collection of minority charge carriers [148]. Most studies reported that a thin layer of p-type emitter for the GaSb TPV cells is feasible to produce good quantum efficiency. Rajagopalan et al. [149] conducted an experimental study to obtain the optimum emitter depth of a GaSb TPV cell fabricated by a single-step diffusion method. The optimum junction depth that produces the maximum power output from the fabricated cell is around 0.4 µm. By decreasing the emitter depth, the quantum efficiency (*QE*) performance of the cell is increased while the V_{oc} is decreased. On top of that, Shaimaa et al. [92] emphasized the trade-off relation between the emitter thickness and the performance parameter, especially with the V_{oc} and J_{sc} values. In this regard, a thick p-doped emitter with a high doping concentration shall therefore decreases the minority carrier lifetime hence decreases the J_{sc} value. Contrarily, V_{oc} is reduced by a thin emitter caused by the increasing leakage current of the cell. Additionally, Bett et al. [150] demonstrated a strong dependency on the quantum efficiency when the emitter thickness was decreased from 0.72 to 0.22 µm in the simulation work. Therefore, the necessity to develop detail optimization with the precise control of the emitter thickness is very crucial.

Recently, Tang et al. [50] performed a doping and depth optimization on a Zn-diffused GaSb cell for both emitter and base regions through simulation work. The doping of both

regions was optimized to increase the *QE* in a range of long wavelengths. For an n-type GaSb substrate, increasing the doping concentration tends to reduce the power output of the cell. As for the p-type GaSb emitter layer, a moderate Zn concentration is sufficient to achieve high *QE*. Optimization on the GaSb structure has been done in recent years. In 2015, Tang et al. [51] performed a numerical simulation to investigate the GaSb cell designed to be an inverted "n on p" configuration through Tellurium diffusion into unintentionally p-doped GaSb TPV cell. The n on "p" configuration with a thin optimal diffusion n-emitter depth of 0.1 μm and a thick p-base shows better performance than the "p on n" GaSb TPV cell configuration. This is because a thick p-base generates a high amount of electron minority charge carriers. In addition, the carrier extraction is improved due to the long diffusion length. Therefore, a higher power density and the *IQE* of the cell were attained in [50,51,151]. Under 1500 K blackbody radiation, the I_{sc} for "n on p" configuration was improved by a factor of 1.43 as compared to the "p on n" GaSb cell configuration.

With regards to the anti-reflective coating (ARC), Fraas et al. [136] discussed the design optimization incorporating an "n+" transparent conductive oxide (TCO) layer with a hydrogenated amorphous silicon interface (Si:H) passivation between the n+ and p-type GaSb base. The integration serves as a built-in plasma filter by reflecting the IR radiation at a longer wavelength back to the radiation source hence improving the overall performance. Recently, Tang et al. [152] demonstrated the n-type vapor diffusion by depositing a silicon oxide layer on the p-GaSb surface. In comparison to a traditional p-on-n GaSb TPV cell structure, higher *QEs* at longer photon wavelengths have been reported, resulting in 1.42 times higher output power density recorded under 1573 K temperature.

Additionally, optimization work has been done on the TPV filter by a research group from Tufts University, USA. Licht et al. [151] demonstrated a 10% improvement in *IQE* with optimized design of a GaSb TPV cell by incorporating a metallic photonic crystal as the front-surface filters (MPhCs). It is claimed that the repeating nanoscale structure of the MPhCs only allows the transmission of near bandgap radiation as this structure creates a photonic bandgap and provides a narrowband confinement of the incident photons. Additionally, the formation of an evanescent field penetrates the GaSb cell results in higher photon absorption. Therefore, MPhCs are coined to reduce various types of recombination mechanisms. Despite all of the advantages, Licht's studies are mainly based on a simulation tool (Silvaco Atlas software), and cell fabrication based on the design structure is yet to be demonstrated and further explored.

5. InGaAs-Based TPV Cell

In this section, a comprehensive study on InGaAs-based TPV cell in terms of their background, cell performance, improvements and challenges are thoroughly discussed.

5.1. Introduction

InGaAs is a III-V ternary semiconductor compound of InAs and gallium arsenide (GaAs) that consists of indium and gallium group III elements, and arsenide group V element. The bandgap energy of InGaAs can be engineered from 1.42 to 0.36 eV by having a variation of x composition in $In_xGa_{1-x}As$, corresponding to cut-off wavelength from 0.87 to 3.34 μm [4]. At x = 0.53, $In_{0.53}Ga_{0.47}As$ is lattice-matched to indium phosphide (InP), corresponds to E_g and λ_c of 0.74 eV and 1.68 μm, respectively. On the other hand, InGaAs cell with a E_g lower than 0.74 eV will have a longer λ_c, this will improve the harvesting of mid-IR and hence increase the output power [153]. A lattice-mismatched InGaAs with higher indium composition is designed to arrive at a lower bandgap. InGaAs cells have the advantage of achieving λ_c up to 2.6 μm. However, the mismatch between the InGaAs and InP substrate results in higher dark current.

In 1980s, Woolf [17] at GA Technologies (San Diego, CA, USA) was the first to propose InGaAs photoconverters for TPV applications. In the 1990s, the National Renewable Energy Laboratory, US (NREL) played a significant role in the collection and promulgation of TPV data, where TPV research on lattice-matched and lattice-mismatched InGaAs were

introduced. Those studies involved the theoretical calculation, growth, fabrication and characterization of InGaAs TPV cells under solar and TPV spectrums. Recently, studies used an InGaAs cell in multi-junction such as GaInP/GaAs/InGaAs [103], and tandem cells such as GaAs/InGaAs [154], which aim to increase the total efficiency and to extend the power harvesting into the mid-infrared wavelengths. Several studies reported the crystal defects of lattice mismatch InGaAs cells for bandgap from 0.55 to 0.6 eV [155], characterization of the cell performances and optimization of the structure design [156–159].

5.2. Performance of InGaAs-Based TPV Cell

Typical lattice-matched $In_{0.53}Ga_{0.47}As$ cell has V_{oc}, I_{sc}, FF and η ranging from 0.3 to 0.4 V, 21.5 to 57.7 mA/cm^2, 66 to 74.2%, and 4.2 to 14.37%, respectively, under AM 0 and AM 1.5 illuminating condition [101–103]. On the other hand, lower bandgap lattice-mismatched InGaAs cells have recently received tremendous attention due to the diversified applications. The indium ratio was increased while the ratio of gallium was decreased to produce a lattice-mismatched InGaAs [160]. Reducing the bandgap of InGaAs will increase the I_{sc} resulting in higher output power. On the other hand, there is a limitation to fabricate a high-performance lattice-mismatched cell which has a lower bandgap on InP substrate. InGaAs with lower bandgaps show a higher degree of Auger recombination, whereas excessive defects due to lattice-mismatched epitaxy cause a high level of Shockley-Read-Hall (SRH) recombination. Both Auger and SRH recombination will increase the dark current and limit the device performance [161]. Recently, Zhou et al. [162] investigated the utilization and optimization of TPV system cavity, which consists of emitter, PV cells, and mirrors to modify the spatial and spectral distribution within the system. It was demonstrated that careful design of the cavity configuration can significantly enhance the performance of the TPV cell.

Moving on, Tan et al. [159] compared the performance of $In_{0.53}Ga_{0.47}As$ and $In_{0.68}Ga_{0.32}As$ cells under blackbody temperatures from 800 to 1323 K. As the blackbody radiation temperature increases, the λ_p of the radiation spectrum gradually shifts to the shorter wavelength. The amount of radiation photons that can be absorbed by the TPV cell considerably increases, leading to higher J_{sc}, V_{oc}, FF and P_{out}. The $In_{0.53}Ga_{0.47}As$ and $In_{0.68}Ga_{0.32}As$ cells obtained an η of 16.4% and 19.1% at 1323 K blackbody temperature, respectively. The η continues to increase as the radiator temperature increases. However, the optimum η cannot be obtained due to the restriction of the blackbody source with a maximum heat temperature of 1323 K. InGaAs cells have shown different performance under TPV and solar spectrums. Cells tested at TPV spectrum have reported higher J_{sc}, V_{oc} and P_{max} when compared to solar spectrum [159,163,164]. The increment in cell performance is related to the illumination intensity of the spectrum, which tends to be higher at TPV spectrum or concentrated solar spectrum [165,166]. On the other hand, lower FF, higher saturation of current density and ideality factor are reported when an InGaAs cell was tested under TPV radiation spectrum as compared to AM 1.5 spectrum. The change in the radiation spectrum has a significant effect on current mechanisms of InGaAs cell, which considerably dominates the minority carriers transport process. Recently, Gamel et al. [165] highlighted the effect of various spectral irradiances (different radiation temperature at different beam intensity) on the performance of TPV cell. The J_{sc} increases linearly with illumination intensity while V_{oc} increases logarithmically. Meanwhile, the FF is expected to reduce with increasing illumination intensity, especially if the physical structure design of the TPV cell does not support the collection of high photogenerated carriers. Such a phenomenon is related to the high resistance losses.

The performance of various single lattice-matched and mismatched InGaAs cells are presented in Table 4. Recently, the growth optimization of high crystal quality lattice-mismatched InGaAs TPV cell has gained considerable attention [156]. The buffer layer plays a key role in developing high-quality lattice-mismatched InGaAs TPV cells. The effect of different buffer structures, such as a single buffer layer, compositionally graded buffer layers and superlattice buffer layers, were investigated [156,167–169]. A lattice mismatch of ~1.2% was introduced

between $In_{0.68}Ga_{0.32}As$ and a compositionally nonmonotonically graded InAsP buffer layer (14 layer grades) [155,156]. On the other hand, Hudait et al. [85,91] has grown $In_{0.69}Ga_{0.31}As$ using the MBE method and reported a 1.1% lattice-mismatch between the device layer and the InP substrate. Recent work by Lian et al. [156] also grew $In_{0.69}Ga_{0.31}As$ using MOCVD method. Under the AM 1.5 spectrum, the J_{sc} and V_{oc} are 47.6 mA/cm^2 and 0.35 V, while the η is 6.9%.

Aside from that, Zhang et al. [177] reported a λ_c at 2.5 µm for $In_{0.8}Ga_{0.2}As$ material, the large lattice-mismatched between the epilayer and substrate cause defect, which affects the quality of the material in both electrical and optical properties. The lattice-mismatched problem was solved using two-step growth methods. Firstly, the thin buffer layer was grown with low temperature. Next, the epilayer was grown with a higher temperature. This approach avoids propagation dislocation, thus improves the crystalline quality of epilayer [91,167–169,177,178]. In summary, extended InGaAs have received attention in photodetector and sensor application, but there is limited work on the characterization of extended InGaAs for TPV application. Therefore, the optimization and characterization of extended InGaAs TPV cells should be systematically carried out to fully exploit their potential in TPV application [177,179].

5.3. Performance Improvements

Research effort towards optimizing the cell performance has drastically increased in the recent years. Optimization on the layer thickness, doping concentrations, as well as Monolithic Interconnected Modules (MIMs) are the major topics reported from various works.

5.3.1. Metal Contact Optimization

Photogenerated carriers in the semiconductor are transferred through the front and back metal contacts, one metal exchanging electrons and the other exchanging holes. For ohmic contact resistance, the n-conductor work function must be much greater than that of the semiconductor, and for a p-conductor much smaller than that of the semiconductor. Under AM 1.5 testing condition, n-p and p-n InGaAs have similar performance due to the long minority carrier diffusion length and good surface passivation [52,164]. However, larger contact resistance in the p-n configuration required a greater surface grid coverage to avoid *FF* loss, leading to much higher shading loss and a significant reduction in efficiency per total area (7.2%) [164].

Ohmic contact formation on InGaAs TPV cell is similar to GaAs PV cell, where the ohmic contact is usually prepared with e-beam evaporation of a metallic multilayer structure in one pump down cycle. For n-InGaAs, the ohmic contact resistance decreases from 10^{-6} down to 10^{-8} Ωcm^2, when the dopant increases from 10^{16} to 10^{19}cm^{-3}. The n-InGaAs has a specific contact resistance $\rho_c = 10^{-7} - 10^{-8}$ Ωcm^2 [180]. For p-InGaAs, higher contact resistance can be achieved as compared to n-InGaAs. The vast majority of lattice-matched and mismatched InGaAs TPV structure reported the use of AuGe and Ti/Au as front metal contact and Au and TiAu as back metal contact [85,102,164] to produce an ohmic contact. Tan et al. [155] used Ni/AuGe/Ni/Au metallization scheme for n-type ohmic contact, and Pd/Zn/Pd/Au metallization was used for p-type ohmic contact. Recently, Kao et al. [132] reported the utilization of AuGe/Au metallization for n-type InGaAs layer. It can be ohmic contact with n+-GaAs and n+-InGaAs contact layers without thermal annealing due to the heavy doping of these layers. Ohmic contact formation between the p-InP substrate and the AuBe/Au metal electrode is an essential factor to improve η up 14.37% by receding the series resistance. Recently, Li et al. [157] proposed Tb/Ni/TiN metal stack for n-InGaAs with lower specific ρ_c of 7.98×10^{-9} Ω cm^2. Increasing the dopant concentration in the Ni-InGaAs alloy and the lowering the barrier height between Ni-InGaAs and n-$In_{0.53}Ga_{0.47}As$ successfully increase the contact resistance.

Table 4. Performance comparison of $In_xGa_{1-x}As$-based TPV Cells.

Structure	Growth Method	T_{rad}	Suns	T_{cell} (K)	λ_c (μm)	Area (cm^2)	V_{oc} (V)	J_{sc} (mA/cm^2)	FF (%)	J_0 (A/cm^2)	P_{max} (mW/cm^2)	η (%)	EQE_{peak} (%)@ λ(μm)	IQE_{peak} (%)@ λ(μm)	Ref
$In_{0.53}Ga_{0.47}As$	MOVPE	AM 1.5	1	n/a	1.7	n/a	0.35	57.7	71.2	n/a	n/a	14.37	~1	n/a	[103]
$In_{0.53}Ga_{0.47}As$	MOVPE	AM 1.5	1	n/a	1.7	0.032	0.39	35.2	71	n/a	n/a	9.72	~1	n/a	[102]
$In_{0.58}Ga_{0.42}As$	MOVPE	Tungsten–halogen	_	303	1.7	n/a	0.405	28.2	69	n/a	n/a	12.4	~90 (1.3)	~99 (0.9)	[164]
$In_{0.62}Ga_{0.48}As$	MOVPE	(3250 K)	_	303	1.7	n/a	0.419	28.8	65	n/a	n/a	12.1	~90 (1.3)	~99 (0.9)	[164]
$In_{0.53}Ga_{0.47}As$	MOVPE	AM 1.5	1	300	1.7	n/a	0.360	42	n/a	6.45 μ	n/a	12.33	n/a	n/a	[159]
$In_{0.53}Ga_{0.47}As$	MOVPE	1323 K	_	300	1.7	n/a	0.22	0.6	57.5	0.067μ	0.06	16.4	n/a	n/a	[159]
$In_{0.53}Ga_{0.47}As$	LPE and diffusion	Tungsten 1800 K	_	n/a	1.7	1	0.465	1000	64	n/a	n/a	~15	90 (0.8)	n/a	[52]
$In_{0.53}Ga_{0.47}As$	MOVPE	AM 0	1	298	1.65	0.09	0.333	39.73	71.6	n/a	n/a	13.3	60 (1.4)	n/a	[98]
$In_{0.53}Ga_{0.47}As$	–	4000 K	_	300	1.7	0.1	0.38–0.44	50–600	69–72.5	n/a	n/a	15–18	n/a	n/a	[170]
$In_{0.53}Ga_{0.47}As$	MOVPE	3300 K	_	300	1.7	0.01	0.291–0.315	181–390	39–40	n/a	20.7– 49.4	4.14 –9.88	n/a	n/a	[171]
$In_{0.68}Ga_{0.32}As$	MOVPE	AM 1.5	1	300	~2	n/a	0.23	56	n/a	1362 μ	n/a	8.06	n/a	n/a	[159]
$In_{0.68}Ga_{0.32}As$	MOVPE	1323 K	_	300	~2	n/a	0.175	10	55	11.6μ	n/a	19.1	n/a	n/a	[159]
$In_{0.69}Ga_{0.31}As$	MOVPE	AM 1.5	1	n/a	2.10	n/a	0.215	47.6	57	n/a		6.9	~1 (80)	n/a	[156]
$In_{0.69}Ga_{0.31}As$	MBE	2050 K	_	298	~2	2.7×10^{-2}	0.357	1180	68.1	n/a	0.2095	n/a	~67 (1.4)	n/a	[91]
$In_{0.68}Ga_{0.32}As$	MOVPE	AM 1.5	1	300	~2	0.0625	0.19–0.23	43–56	n/a	n/a	n/a	5.31 –8.06	n/a	n/a	[155]
$In_{0.69}Ga_{0.31}As$	N/A	AM 0	5.7–27.2	298	~2	0.13	0.27–0.38	45	~66.3 –71.3	443 n	(0.13–3.42) × 10^2	5.4–7.8	75 (1.5)	n/a	[166]
$In_{0.69}Ga_{0.31}As$	MBE	1920 K–2050 K	_	298	~2.1	2.82×10^{-2}	0.334–0.355	(1.11–2.26) × 10^3	65.6–66.5	7.2×10^{-4}–3.3 x10^{-5}	0.195–0.532	n/a	100 (1.2)	n/a	[85]
$In_{0.68}Ga_{0.32}As$	MOVPE	infrared lamp illumination	0 _ 72 V	293	~2.05	n/a	0.38	1.7×10^3	70	n/a	0.25×10^3	n/a	82 (1.2)	n/a	[73]
$In_{0.72}Ga_{0.28}As$	MOVPE	tungstenhalogen light	_	n/a	~2.2	1	0.291–0.301	(3–3.7) × 10^3	n/a	0.07–1	n/a	n/a	56.7 (2)	n/a	[172]
$In_{0.72}Ga_{0.28}As$	n/a	1273–1773 K	15 Wcm^{-2}	300	~2.2	n/a	0.317–0.332	(3.87–7.08) × 10^3	48.7–57.7	n/a	0.71–1.15	4.7–7.6	n/a (1.9)	n/a	[163]
$In_{0.72}Ga_{0.28}As$	n/a	n/a	n/a n/a	300	~2.2	1	0.28–0.32	(1–4) × 10^3	54–65	2×10^{-5}	0.18–0.58	n/a	88 (1.6)	n/a	[173]
$In_{0.72}Ga_{0.28}As$	MOVPE	n/a	n/a	n/a	~2.2	1	0.298 –0.31	(1.1–1.2) × 10^3	62–65	n/a	n/a	n/a	~70 (1.5)	n/a	[174]
$In_{0.78}Ga_{0.22}As$	PECVD	1273 K	n/a	298	2.4	n/a	0.307	3.65×10^3	59.8–63.2	56–1330 μ	n/a	n/a	n/a	~2.2 (99)	[175]
$In_{0.79}Ga_{0.21}As$	MOCVD	1273 K	n/a	298	~2.5	1	38	26.3	n/a	n/a	0.2	n/a	n/a	n/a	[176]
$In_{0.83}Ga_{0.17}As$	MBE	n/a	n/a	300	~2.65	n/a	n/a	3.7×10^{-3}	n/a	n/a	n/a	n/a	n/a	n/a	[177]

5.3.2. Thickness, Doping and Design Structure Optimization

The variation of layers' thickness and doping concentration directly affect the output performance of InGaAs TPV cell. For example, the increment of absorber thickness will increase the J_{sc} as more photons are absorbed. On the other hand, V_{oc} decreases with the available length over which carriers' recombination can occur. Moreover, doping density will significantly affect the lifetime and mobility of carriers. Finding the optimum thickness and doping concentration of InGaAs TPV cell will maximize its output performance [102,103].

Most of the literature reported a very thin layer of emitter layer from 0.1 to 0.3 µm [155]. Thinner highly doped emitter is able to produce lower resistance depending on the metal contact and able to generate a feasible electric field with the base layer. Aydin et al. [158] reported an optimum thickness (doping concentration) of 0.5 µm (1×10^{17} cm^{-3}) for emitter layer and 3.5 (1×10^{17} cm^{-3}) for a base layer under 1400 K blackbody radiation. Emrnzian et al. [171] used PClD software to optimize the thickness and doping concentration of the emitter and base layers of $In_{0.53}Ga_{0.47}As$ under 0.5 W/cm^2 at 3300 K blackbody temperature. Optimum cell performance is reported at base and emitter thickness of 2 µm and ~0.2 µm. In [170], the doping concentrations and thicknesses of the emitter and base layers of $In_{0.53}Ga_{0.47}As$ TPV cell were optimized under 2000 K and 5000 K blackbody temperatures. It was reported that J_{sc} and η steadily improve as the base thickness increases from 0.5 to 2 µm, but the increasing trend saturates as thickness further increases beyond 2 µm. Emitter thickness <0.3 µm and doping concentration of ~1×10^{17} cm^{-3} provide optimum device performance. Under 2000 K and 5000 K blackbody temperature, 0.3 µm and 3×10^{17} cm^{-3} for the emitter, and 2 µm and 1×10^{17} cm^{-3} for the base were reported [170]. Recently, Gamel et al. [181] reported a multi-dimensional optimization of $In_{0.53}Ga_{0.47}As$ TPV structure using the real coded genetic algorithm at radiation temperatures between 800 to 2000 K. Cell efficiency increased by an average percentage of 11.86% as compared to the non-optimized cell. It was highlighted that the integration of a thicker base layer with the back-barrier layers enhance the generation of charge carriers and increases the collection of photogenerated carriers near the band-edge.

The majority of InGaAs devices are epitaxial grown heterojunction. The active junction is combined with cap, window, buffer layers, which play an important role in improving device performance. A very thin and heavily doped InGaAs cap layer <1×10^{19} cm^{-3} obtains a low resistance (Ohmic contact) with the front metal contact and selectively removed except at the contacts to avoid optical absorption by the cap layer [102,166]. Jain. [182] investigated the effect of p-InP window layers for lattice-matched $In_{0.53}Ga_{0.47}As$ cells using PC1D software. The *EQE* results demonstrated the suitability of window layer to reduce front surface recombination resulting in a significant improvement. The large conduction band discontinuity at the window/emitter interface provides a tremendous potential barrier for the movements minority carriers and reduces the surface recombination of electrons. It was found that under AM 1.5, devices with 1.5 µm window layer produce lower J_{sc} as the majority of light spectrum is absorbed by InP layer. For TPV application, significant portion radiated energy will be lower than E_g of InP. The R_s value can be further minimized by optimizing the physical parameters (doping and thickness) of the entire structure. Ming et al. [155] presented an improvement in TPV device for an $In_{0.68}Ga_{0.32}As$ cell with optimized material growth, suitable absorber thickness of 2.8 µm as well as TiO_2/SiO_2 ARC with 2.1 µm InAsP buffer layer. Such enhancement has increased the V_{oc} from 0.19 to 0.23 V, the J_{sc} from 43 to 56 mA/cm^2, and the conversion efficiency from 5.31 to 8.06% under AM 1.5 test condition. Research focuses on single-variable optimization to improve on the TPV cell η, the research gap that worth to be highlighted is to perform multi-variables optimization to achieve a higher cell η.

5.3.3. Advancement and Improvement in InGaAs TPV Cell

For TPV cells improvement-wise, optimizing the ARC materials and thickness play a key role in decreasing the reflection at the front surface of the InGaAs cell. Other methods like the rear mirror reflector, Lambertian rear reflector and textured surface are used to

improve the light absorption and light trapping in the cell [183]. Jurczak et al. [184] investigated the effect of ambient temperature and light trapping (rear reflector and textured surface) on the performance of InGaAs using Matlab. Results show a 3–5% improvement when the light trapping is implemented. Recently, Burger et al. [185] suggested the potential for a dramatic increase in conversion efficiency through improved spectral selectivity and recycling of longer IR, combined with the potential for reduced module costs through wafer reuse using thin-film TPV. The air-bridge InGaAs thin-film device with gold rear mirror reflector was investigated to realize highly selective absorption of above-bandgap radiations, enabling more efficient photon recycle and improving the TPV performance. Thin-film exhibits higher average sub-bandgap reflectance of 99% comparing to <95% sub-bandgap reflectance of conventional cell. The simulation suggests a TPV cell exhibiting these properties operates with an efficiency above 30% with 1455 K SiC radiator. Other method suggested the use of a closed system chamber which combined the radiator and InGaAs with near mirror reflector. The illumination reflected from the rear reflector recycled back in the radiator creating light trapping TPV system. Such improvement makes it possible to achieve system efficiency >50% [186].

Monolithic interconnected modules were implemented for the TPV system to improve the system efficiency [187]. MIM provides several advantages, firstly is that series-connected cells generate high voltage and low current, the array size can be designed to minimize the loss due to non-uniform radiator temperature. Also, the MIM cell can be directly connected to the substrate or heat sink without any electrical isolation limitation concern [188]. The lattice-matched InGaAs/InP MIM of 0.74 eV bandgap energy and lattice-mismatched MIM of 0.55 eV bandgap were studied [189]. Fifteen InGaAs cells in series connection with an active area of 0.9 cm $\times$ 1 cm were tested, and a gold BSR was recommended for efficient radiation recuperation. The literature shows that InGaAs MIM TPV cell with 0.74 eV recorded V_{oc} of 6.16 V, FF of 0.74 and J_{sc} of 0.84 A/cm^2, while InGaAs MIM TPV with 0.55 eV recorded V_{oc} of 4.85 V, FF of 0.58, and J_{sc} of 3.87 A/cm^2 [189]. This study shows that series connected MIMs generate high voltage and low current. The reliability of MIMs could be further improved by designing series-parallel string MIMs. Moving on, Wehrer et al. [190] further explored the TPV tandem converter technology to improve TPV efficiency while sustaining high power densities. The study was conducted on an epitaxial grown lattice-matched $In_{0.53}Ga_{0.47}As$ with 0.74 eV bandgap energy and lattice-mismatched $In_{0.64}Ga_{0.36}As$ with 0.63 eV bandgap energy. Under a 1273 K of blackbody source radiation and 325 K of cell temperature, V_{oc} of 6.14 V, I_{sc} of 0.292 A/cm^2, and FF of 0.676 were attained [190].

Other improvements are presented by matching the radiation spectrum to the spectrum response of InGaAs devices. Woolf et al. [191] reported 43% and 52% of spectral efficiency at 1300 K and 1500 K for $In_{0.68}Ga_{0.32}As$ TPV cell with cell efficiency of 22% and 26%. In 2017, David et al. [17] presented the novel selective thermal radiator to improve the efficiency of TPV system with source temperature above 1000 °C and a $In_{0.68}Ga_{0.32}As$ TPV cell. Using the conventional stepper lithography, the radiator was produced using a passivated platinum and alumina frequency selective surface. A power conversion efficiency of 24.1% was achieved at 1055 °C of radiation temperature with spectral efficiency of 80%. In 2018, Fekadu et al. [48] numerically analyzed a multilayer optical radiator based on metamaterial design which exhibited polarization and azimuthal angle independent selective emission for $In_{0.68}Ga_{0.32}As$ TPV cell. The proposed multilayer TPV cells achieved an enhanced broadband and a wide-angle average emissivity of 96.6% between 0.2 to 2.1 µm. Spectral efficiency of 79.6% was achieved for TPV cell at λ_c of 2.1 µm under 1400 K source energy as compared to 56.6% for a single layer. Recent improvement in the TPV cells and system improve the conversion efficiency and output power, hence increases the feasibility and practicality of TPV in various terrestrial and space applications.

6. Narrow Bandgap Materials for TPV

TPV cells utilize narrow bandgap materials which allow them to harvest the maximum amount of infrared radiation. Aside from the available TPV materials: GaSb TPV cell discussed in Section 4 and InGaAs TPV cells in Section 5, there are several narrow bandgap materials that worth highlighting. Single element semiconductor like Ge with a bandgap of 0.66 eV, binaries like InAs with a bandgap of 0.35 eV and indium antimonide (InSb) with a bandgap of 0.17 eV and ternary like indium gallium antimonide (InGaSb) with a bandgap energy range of 0.17–0.72 eV and indium arsenide antimonide (InAsSb) with a bandgap energy range of 0.1–0.4 eV and quaternary like InGaAsSb with a bandgap energy range of 0.5–0.55 eV and InAsSbP with a bandgap energy range of 0.3–0.5 eV are accessible narrow bandgap materials. There are several types of potential TPV materials as listed in Table 5, yet with some limitations and room for improvement in terms of TPV cell optimization and light trapping. These materials can be further explored for the potential to harvest waste heat temperature below 1200 K.

Theoretically, TPV cells made by narrower bandgap semiconductors are able to absorb photons up to longer wavelengths, resulting in better cell performance. However, there are several drawbacks of narrow bandgap (<0.7 eV) TPV cells such as low V_{oc}, high dark current, and immature growth technology, and nonoptimal structure design. Recently, Gamel et al. [192] compared the performance of various reported narrow bandgap cells under 1000 K blackbody temperature. Based on their simulation result, $In_{0.53}Ga_{0.47}As$ has better *IV* curve characteristic in comparison to Ge, GaSb and InAs, due to the mature structure with FSF and BSF layers which results in lower surface recombination. InAs with the long λ_c of 3.5 µm produced an output power of 36.7 mW/cm^2 as compared to 42.1, 27.7 and 6.3 mW/cm^2 produced by $In_{0.53}Ga_{0.47}As$, GaSb and Ge cell, respectively. Furthermore, InGaAsSb is more promising as compared to GaSb and Ge, due to the high cell efficiency and its ability to operate in the low range blackbody temperature. Furthermore, Table 5 and Figure 3 summarize and compare the characteristics of narrow bandgap materials for TPV cells. Based on the comparison in Table 5, aside from extended InGaAs, InGaAsSb has the best potential among the narrow bandgap materials for radiation low-temperature (<1273 K) due to its promising V_{oc} and J_{sc}, yet further cell optimization is needed to improve the cell efficiency. Based on the current literature, InAsSbP TPV cell has limitation in achieving a promising *FF* and V_{oc}, with epitaxial and diffusion emitter, the V_{oc} recorded at 0.1 V [193]. InGaAsSb and InSb are therefore worth to be further optimized and improved for TPV application. Furthermore, as illustrated in Figure 3, InGaAs (0.74 eV) and GaSb TPV cells recorded the highest cell efficiencies, which demonstrates the maturity of these structures.

Table 5. Narrow Bandgap Materials TPV cells.

Ref	Material	T_{rad}	T_{cell} (K)	λ_c (μm)	E_G (eV)	V_{oc} (V)	I_{sc} (A)	J_{sc} (A/cm^2)	FF (%)	η_{cell} (%)	Exp./ Sim.
[194]	Ge	AM 0	300	1.9	0.66	n/a	n/a	n/a	n/a	13	Exp
[195]	Ge	2000 K (3.66–36.6 W/cm^2)	300	n/a	0.664	0.323–0.383	5×10^{-7}–5.1×10^{-6}	n/a	73.4–76.4	9.6–11.9	Sim
[196]	Ge	AM1.5 × 25 sun	298	~1.6	0.6	0.34	0.89	n/a	68	28.8	Exp
[197]	$In_{0.2}Ga_{0.8}Sb$	AM 1.0	N/A	2.2	0.56	0.24	n/a	0.037	n/a	34.33	Sim
[198]	$In_{0.2}Ga_{0.8}As_{0.17}Sb_{0.83}$	1800 K	300	2.4	0.53	0.35	n/a	36.3	n/a	16.2	Sim
[63]	$In_{0.15}Ga_{0.85}As_{0.14}Sb_{0.86}$	1470 K	300	2.4	0.53	0.327	n/a	3.01	65	20.92	Exp
[59]	InGaAsSb	1100 K	N/A	~2.4	0.53	-.18		0.5	n/a	n/a	Exp
[199]	$In_{0.16}Ga_{0.84}As_{0.14}Sb_{0.86}$	1500 K	300	2.44	0.506	0.3–0.5	n/a	50	65	10	Sim
[200]	$In_{0.25}Ga_{0.75}Sb$	1200K	300	2.5	0.50	0.34	n/a	3.2	n/a	22	Sim
[62]	$In_{0.22}Ga_{0.78}As_{0.2}Sb_{0.8}$	1328 K	300	~2.5	0.49	0.187–0.231	n/a	1.042–2.170	44.2–46.9	n/a	Exp
[62]	$In_{0.22}Ga_{0.78}As_{0.2}Sb_{0.8}$	1328 K	300	~2.52	0.49	0.208–0.240	n/a	6.895–8.815	51.3–54.9	n/a	Sim
[78]	$Ga_{0.78}In_{0.22}As_{0.20}Sb_{0.80}$	AM 1.5 and 1073 K	N/A	~2.52	0.50	0.074 and 0178	n/a	0.035 and 0.98	33 and 46	n/a	Exp
[201]	Cascade InAs/GaSb/AlSb	800 K	300	3.1	0.40	0.799	17.9 m	43.5	51.4	9.6	Exp
[202]	InAsSbP	AM 1.5	N/A	3.5	0.39	0.12	n/a	3	n/a	n/a	Sim
[203]	InAs	1223 K	300	3.5	0.35	0.06	n/a	0.9	n/a	n/a	Exp
[204]	InAs	1073 K	300	n/a	0.36	0.027	n/a	0.267	27	0.61	Sim
[205]	$InAs_{0.91}Sb_{0.09}$	800–1400 K	300	4.33	0.286	0.83–0.154	n/a	1.9–30	n/a	8–16	Sim
[206]	InSb	773 K	300	n/a	0.235	n/a	n/a	n/a	n/a	n/a	Sim
[207]	InSb	1273 K	300	n/a	0.235	0.085	10×10^{-6}	n/a	64	n/a	Exp

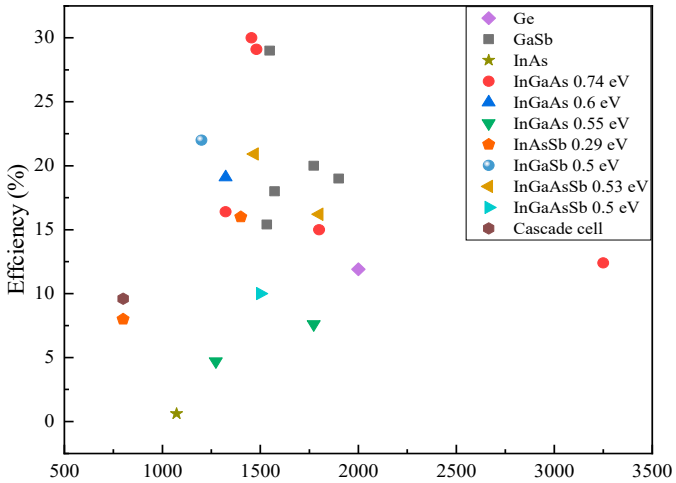

Figure 3. Record TPV cell efficiencies for various materials Ge [195], GaSb [3,131,134], InAs [204], InGaAs [52,103,159,163,185,186], InAsSb [205], InGaSb [200], InGaAsSb [63,198,199] and cascade InAs/GaSb/AlSb [201].

7. TPV Applications

TPV system received tremendous attention due to its promising contribution as economical, efficient, practicable power systems, and clean power generation. The application of TPV can be categorized based on the chemical reaction or nuclear fusion reaction types of thermal heat source. These heat sources are categorized into solar heat, combustion of fuels, nuclear sources and waste heat. Figure 4 presents the application for TPV technology.

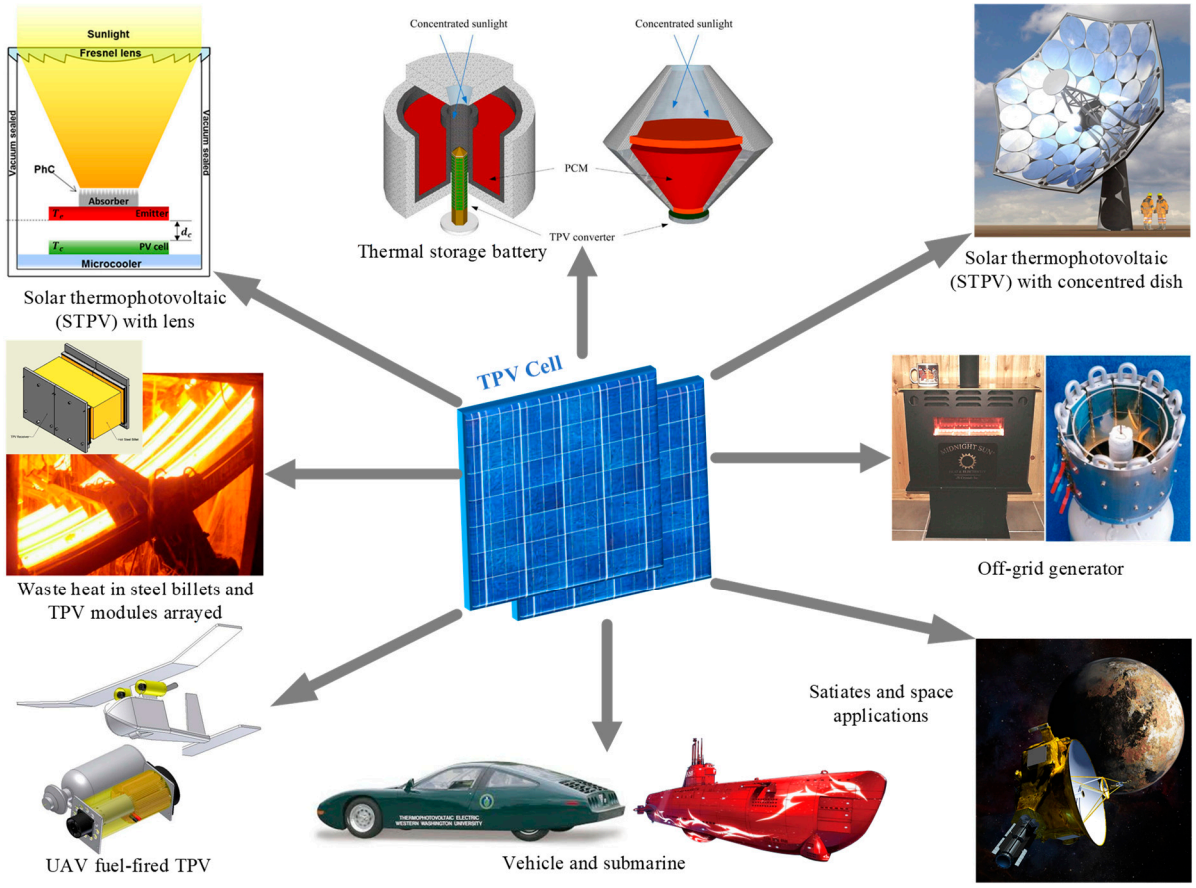

Figure 4. TPV applications.

7.1. Solar TPV Systems (STPV)

In principle, STPV system utilizes the solar energy to heat up the radiator to <3273 K through a solar concentrator. These high-temperature radiators will then emit thermal radiation to the TPV cells that converts the infrared photons into electricity [208]. STPV work has been reported on Fresnel point-focus and dish concentrators, which recorded a temperature up to 1623 K [4]. Xuan et al. [208] emphasized that the configuration of radiators influences the distribution effect of radiator temperature. A cylindrical radiator was found to give the most stable performance for STPV system. Zhou and associates [209] performed a comprehensive review of TPV cells material in STPV system. In contrast to Si and Ge cell, GaSb and InGaAs TPV cells show better performance in STPV system. Nevertheless, the cost of material and fabrication process remain a big challenge. Furthermore, a multi-bandgap cell such as GaInP/GaAs/Ge shows the potential of integration into a STPV system, which possesses higher conversion efficiency as compared to a single junction cell [4]. Nowadays, the STPV system in a hybrid system attracts considerable interest. Hussain et al. [210] conducted a performance analysis on different arrangement of hybrid STPV design using solar-biomass/gas power generation system. The hybrid STPV system can be operated at temperature lower than 1273 K, which widens the opportunity for other applications such as portable battery charger and microgenerator for household application. In addition, STPV hybrid with solar-natural gas has been demonstrated to give an electrical power output around 500 W and a conversion efficiency of 22% [211]. This architecture offers a promising development in the near future.

7.2. Combustion-Driven TPV Generators

Combustion-driven TPV system can be widely considered for micro-, meso-, and macro-scale power supply applications [212]. Practical applications of combustion-driven TPV generator include portable electric generator, combined heat and power (CHP) as well as hybrid electrical vehicles. Portable TPV system was highly recognized in military application, aiming to replace heavy batteries and noisy diesel-electric generators [2]. Collaboratively, JX Crystal Inc. developed the first hydrocarbon-fueled TPV generators using GaSb TPV cell known as "Midnight Sun", producing electrical power up to 100 W [121]. McDermott Technology Inc (MTI) has then teamed up with JX Crystal and developed a 500 W diesel-fueled portable TPV power generator. In addition, Chan et al. [213] developed a portable microgenerator with the combination of propane-fueled TPV microgenerator, photonic crystal radiator, and low bandgap InGaAs-based TPV cells. After a thorough system analysis, Chan et al. [214] redesigned the micro burner and developed vacuum packaging to prevent convective loss to the photonic crystal. Results suggested that further development can be promoted for higher conversion efficiency. For home-scale operation, this technology is often called the off-grid generator where the system aims to provide heat and electricity to remote houses during the winter and night time.

The CHP-based TPV has not only been realized to provide good performance for home use, but the system is also applicable in larger scale such as the central heating furnaces in large buildings and industrial furnaces [215]. Limitation of TPV system in CHP is the low-grade heat generation due to heat dissipation during the cooling of TPV cells. The typical cell temperature in CHP mode is around 333 K, which has been suggested with an additional heat exchanger to upgrade the heat for the exhaust gas [4]. Exploitation of micro-CHP has been investigated on domestic boilers in residential area to provide central heating which converts waste heat into electricity [216]. Bianchi et al. [217] investigated CHP TPV for residential buildings, considering both the energetic and economical point of view. In addition, low bandgap tandem cell such as InGaAsP/InGaAs shows the potential of incorporation in CHP systems. In comparison to thermodynamic limit, a significant improvement was made for lower bandgap materials on the TPV cell conversion efficiency [218]. De Pascale et al. [219] introduced a thermodynamic analysis of CHP by integrating a TPV generator into an Organic Rankine Cycle. A 56% thermal efficiency and 24% electrical efficiency were achieved in optimum electrical load configuration.

In hybrid electric vehicle (HEV), the exhaust heat from gas-powered engine is converted by a TPV device to charge the batteries with sufficient power to accelerate and maintain a cruise speed. TPV generators which produce a power range from 6 to 10 kW were investigated for HEV [122,123]. The major concern for TPV generators in HEV is the requirement of high efficiency. For instance, a 10 kW output capability is needed to maintain a steady-state cruising at 113 km/h without drawing any power from the battery [122]. The first TPV-powered automobile prototype was built in 1999 and named as "Viking 29" [123], which utilized GaSb-based TPV cells. The TPV generator consists of 20 GaSb-based TPV cells connected in series and V_{DC} of 126 V [122]. The challenge of low conversion efficiency for the currently available TPV systems would be more reliable to support a small vehicle with smaller power range [2]. Research efforts have been devoted towards future development for better heat recovery and improvement of the system efficiency to achieve high-performance HEVs. The design system with selective emitter and quantum well TPV cell theoretically capable of yielding 24.5% of efficiency and 6 kW of electric power to recharge the battery pack of an electric city-car. However, further experimental investigations are needed for the emitter-cell system [26].

7.3. Space Applications

Moving forward, high-efficiency TPV cells are essential in space technology application [4]. There are two feasible power sources to power up a small spacecraft for long duration, which are solar and nuclear generators [220]. Recently, a critical review was conducted on space power generation to compare the main competing technologies [10]. TPV system promises up to 40% of efficiency and additional advantages of lightweight, mechanically static, and direct electricity production from radiant heat in space power generation. Also, the TPV system generates high power density per unit area as compared to other technologies, which is suitable for medium electrical system. The power density can be further increased with the use of radioisotope TPV generators with the use of nuclear fission sources [220,221]. For nuclear generators, the heat range is typically from 10 kW to MWs [222], and these generators are currently under consideration for power generation in future planetary settlement missions [10]. The most recent development of RTPV has been made in the Institute for Soldier Nanotechnologies [223,224] where simulation and measurement results have been experimentally reported on RTPV prototype system using photonic crystal spectral control in terrestrial application. Moreover, a RTPV system designed with InGaAsSb cell was reported with 8.26% efficiency and output power of ~40 W [225,226]. A 0.6 eV InGaAs TPV cell is very useful in the space application with less than 1% of cell degradation in performance over years caused by the damaging effect in the system. The Plutonium-238 radioisotope was investigated with up to 3 W power output and 10% system efficiency at the Los Alamos National Lab [227].

7.4. Waste Heat Recovery (WHR)

Effort has been made by researchers and private companies in exploring the possibility of utilizing TPVs for power generation [228–230]. In the UK industrial activities, the potential of TPV system to recover waste heat was realized in high-temperature industry [228]. Turkish industrial sectors [125,230] estimated that the potential energy recovery using TPV system is around 22.40 to 67.45 PJ/year. Moreover, a recent thermodynamic analysis of TPV system for industrial WHR application reported that up to 7.31% of annual waste energy can be recovered [15]. Despite the great promise of a TPV system in the WHR application, low power conversion efficiency at waste heat temperature less than 1273 K has been a major concern [229]. This can be solved by implementing TPV cells with material bandgap lower than 0.7 eV such as InGaAs and InAs. Furthermore, the potential of TPV heat recovery in glass and steel manufacturing industry have been an attractive research area nowadays. In glass manufacturing industry, the TPV system is estimated to produce 270 kW power output from high-temperature object with a surface area of 27 m^2 [231]. In addition, Fraas et al. [3] successfully demonstrated a TPV cell with power density output

of 1.5 W/cm^2 per cell generated from a hot glowing radiant tube burner (1548 K) at a steel industry. Besides, the potential of worldwide electricity production is estimated with the possibility to reach over 3.1 GW with TPV heat recovery system in steel industry.

7.5. Thermal Energy Storage System

TPV devices are of particular interest for thermal energy storage application. Conceptually, thermal energy storage system utilizes ultra-high temperature phase change materials (PCM). In this system, the energy is stored in the form of latent heat and transformed to electricity upon demand via TPV cells. Thermal storage system enables an enormous thermal energy storage density of ~1 MWh/m^3, which is 10–20 times higher than that of lead-acid batteries, 2–6 times higher than Li-ion batteries as reported by Datas et al. [232]. Seyf and Henry [233] modelled a thermal energy storage system and identified the significant design parameters that affect the overall power cycle system efficiency. It was found that building systems at sufficiently large scales, integrating an effective BSR, increasing the *EQE* for photons above the bandgap will improve the system performance. Following that, the multi-junction or multiple TPV cells arranged optically in series can reduce the thermalization losses and may have the potential to exceed the efficiencies of combined cycles (~60%). In 2019, Amy et al. [234] employed ultra-high temperatures and multi-junction photovoltaics (2-junction cells) for thermal energy storage system. This new approach has several benefits including the ability to reach >50% roundtrip efficiency with a cost per unit power < $0.5 per W-e, and the potential to offer load following capabilities to grid operators.

8. Challenges and Recommendation

The market penetration of TPV system remains inconclusive due to the great challenges encountered throughout its technological development. In the next ten years, TPV technology is expected to become stable and technologically matured such that it is able to produce high power density output for future electricity generation. In this section, the issues and challenges in TPV technology on the overall TPV system, GaSb-based and InGaAs-based TPV cells are extensively discussed, together with the recommendation to overcome the challenges.

8.1. Spectral Mismatch to the Bandgap of TPV Cell Material

In principle, TPV cells operate at the optimum efficiency when the semiconductor energy bandgap is spectrally matched to the blackbody spectrum generated by the heat source [4]. Therefore, TPV cells material shall be chosen based on the bandgap, which correspond to the spectrum. This is to minimize optical loss cause by the spectral mismatch and poor absorption of photons by the TPV cell.

Tan et al. [159] compared the performance of $In_{0.53}Ga_{0.47}As$ (0.74 eV) and $In_{0.68}Ga_{0.32}As$ (0.6 eV) under various range of blackbody temperatures. It was found that the efficiencies of both cells gradually increased from 800 to 1323 K. The key reason for the efficiency increment is due to the positioning between cut-off wavelength of the materials and the peak emissivity (λ_p) of each temperature. As the temperature increases from 800 to 1323 K, the λ_p shifts to a longer wavelength. At 1323 K, $In_{0.68}Ga_{0.32}As$ records 3.3% higher efficiency as compared to $In_{0.53}Ga_{0.47}As$. The reason is because $In_{0.68}Ga_{0.32}As$ (2.10 μm) has a nearer λ_c with λ_p at 1323 K (2.19 μm), in comparison to $In_{0.53}Ga_{0.47}As$ (1.68 μm). The conversion of electricity effectively occurs at photon wavelengths near the λ_c of a particular material. Assuming the highest photon-electricity conversion is achieved when λ_c is approximately similar to the λ_p, the suitable operating temperature as a function of bandgap energy can be expressed by Equation (5).

$$\lambda_c \approx \lambda_p \frac{hc}{E_g} \approx \frac{2900}{T_{BB}} T_{BB} \approx \frac{2900}{1.240} * E_g \quad (5)$$

In this study, the suitable operating temperature for a particular material is suggested to be ± 10% of the λ_p, as illustrated in Figure 5. For instance, the suitable temperature for InSb computed using equation 5 is approximately 397.58 K, which equivalent to λ_p = 7.294 µm. A ± 10% of the λ_p will give 6.5646 µm ≤ λ_p ≤ 8.0234 µm, which corresponds to 361 K ≤ T_{BB} ≤ 442 K.

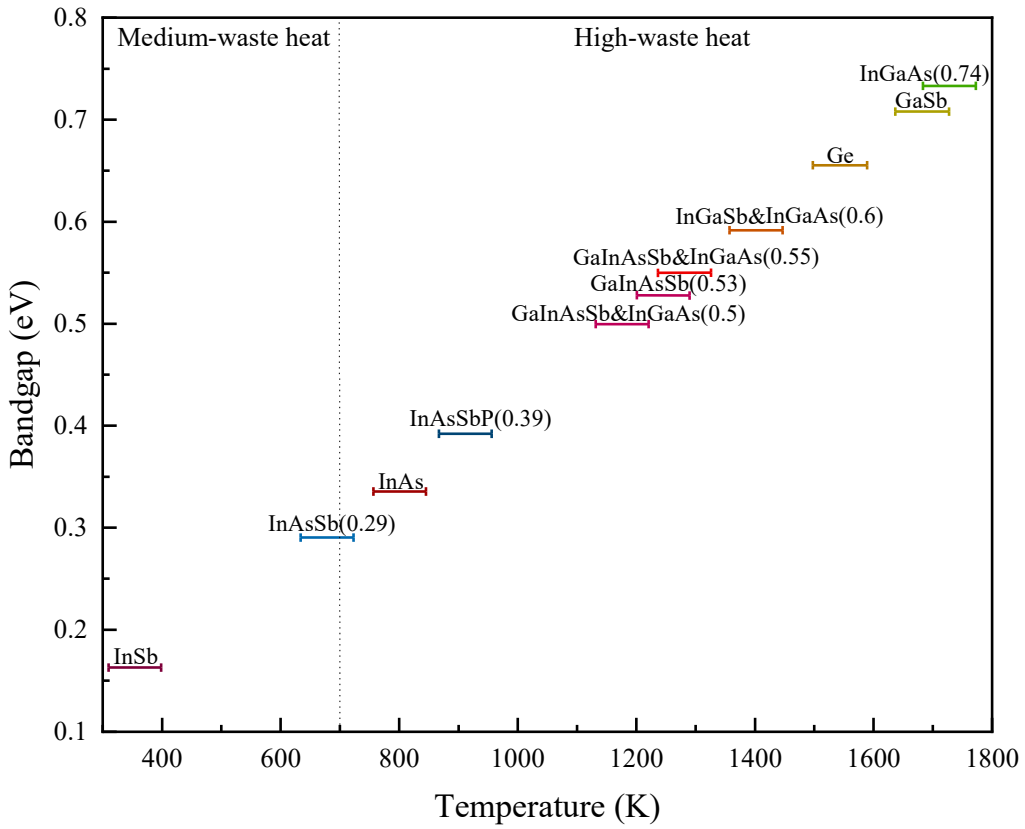

Figure 5. TPV cells and the blackbody temperature range of their optimum performance.

Figure 5 shows that higher source of temperature is desirable for material with a higher bandgap energy. While InSb (E_g = 0.17 eV) operates under lower range of blackbody temperature from 361 to 442 K, a lattice-matched InGaAs TPV cell (E_g = 0.74 eV) operates at a blackbody temperature of 1600 to 1850 K. Furthermore, TPV cell can be matched with the emissivity of the practical radiator. Selective radiators can be engineered to emit at setting range of IR. In short, mismatching between the heat source spectrum and bandgap of the cell is one of the considerable issues that usually causes lower output energy and reduces the efficiency of TPV system. Therefore, the matching of blackbody spectrum to the suitable range of TPV cell bandgap energy is essential to generate the optimum amount of energy per unit area. The reflection and recycling of sub-bandgap photons in the radiator will significantly enhance the conversation efficiency of the TPV system.

8.2. The Effect of Cell Temperature

The TPV cells typically operate at temperature higher than 300 K and is located near to the heat radiator to achieve maximum light intensity. Since TPV cell is exposed to constant thermal radiation during its operation, the cell may heat up to a certain degree that may directly affect the cell performance [235]. Nevertheless, the increment of TPV cell temperature increases the J_{sc} due to the reduction in the bandgap energy of semiconductor material. The decrease in E_g allows more photons at slightly longer wavelength to be absorbed and

create additional electron-hole pairs. The Varshni's semi-empirical relation describes the effect of temperature on the bandgap energy as expressed in Equation (6) [236].

$$E_g(T) = E_{g0} - \frac{aT_{cell}{}^2}{T_{cell} + b} \quad (6)$$

where E_g *(T)* is the engineered bandgap at the setting cell temperature, T_{cell} is the cell temperature, E_{g0} is the initial bandgap at room temperature, b is the room temperature in *Kelvin*, and a is the temperature coefficient.

However, the V_{oc} decreases with an increase in cell temperature [237]. For example, Martin and Algora [235] reported that a GaSb TPV cell has an absolute temperature coefficient for V_{oc} of -1.59 mV $^{\circ}C^{-1}$. Another factor of the decrease in V_{oc} is that the dependence of the dark saturation current on the intrinsic concentration (n_i). The n_i changes due to the E_g dependence on the temperature. Therefore, when the E_g reduces as temperature increases, higher n_i will lead to higher dark saturation current, resulting in the lower V_{oc}.

The challenge of increased internal temperature of the TPV cells can be addressed by several methods. Apart from the incorporation of radiator and filter to protect the cell from thermalization effect, active cooling systems such as heat sinks, cycling coolant and forced-air coolant are commonly employed in numerous TPV prototypes [238]. Wu et al. [41] experimentally illustrated the integration of water-cooled mechanism in TPV system. The cooling system was operated using tap water, water flows through a series of parallel channels. On the other hand, coating the bottom of aluminum chassis heat sink with an additional thermal radiation layer has been demonstrated to enhance thermal radiation in concentrated solar cell by reducing 10 °C of the cell temperature [239]. A setup of cooling system for TPV applications using low-iron soda-lime glass was studied with opto-electro-thermal coupled simulation by Zhou et al. [240] to investigate the effect of temperature under different condition for the TPV application. Subsequently, further experimental work is required to examine this system in practical condition. The integration of TPV with PCM such as paraffin wax, graphene, nano-PCM [241] will lead to an effective cooling and thermal energy storage TPV system. Furthermore, separating the cell from the radiator by transparent insulator layer or undoped semiconductor layer will help to protect the TPV cell from the hot radiator. It would also reduce the cell temperature by means of lower conduction and convection heat transfer to the cell.

8.3. Cost-Effectiveness of TPV Cell Commercialization

One of the major challenges in TPV application is to develop lower-cost of commercialized TPV cells. Some of the TPV structures are fabricated using expensive growth technology such as MBE. Additionally, most TPV cells require front and back surface field layers to optimize cell performance. These layers enhance the collection of long and short photogenerated carriers [242]. Hence, expensive epitaxial growth is employed in the deposition process of these layers.

Lattice-matched TPV substrate is another issue that makes the TPV production cost-ineffective. This is because the production of thick TPV substrate is expensive, which makes the fabrication of thin substrate in sub-micron scale a challenging issue. Therefore, the incorporation of commercially available and cost-effective substrates to grow TPV cells is a significant solution to address the high fabrication cost of TPV cells. For instance, growing a GaSb layer on GaAs substrate is a lower cost option as compared to GaSb substrate. Currently, ELOG method is used to grow GaSb junction on GaAs substrate with low mismatch defect [77]. Therefore, research on integrating ELOG method in different TPV materials will be an interesting research topic. Furthermore, the combination of Zn diffusion and epitaxial growth method was reported for InAsSbP/InAs p/n junction on InAs substrate by Krier et al. [65]. The combination allows higher cell performance due to low surface recombination. Further investigation for other types of TPV materials that could potentially reduce the economical barrier for mass scale TPV production is needed.

On top of that, Ge with a bandgap of 0.66 eV is a cost-effective candidate for the fabrication of TPV devices. Ge structure can be easily deposited on either Ge or GaAs substrates. However, the cell efficiency of Ge is lower than those of GaSb and InGaAs TPV cells. This is attributed to its higher density of states in the conduction band caused by the high electron mass as a consequence of high dark current, low V_{oc} and high-temperature coefficient [202]. In addition, the quality of the Ge crystal with indirect bandgap tends to induce the recombination rate in the TPV cell, which decreases the overall efficiency. A number of studies have been conducted to improve the performance and to reduce the fabrication cost of Ge cell. For example, amorphous silicon (a-Si:H) was demonstrated to create a surface passivating material for Ge [243]. This structure generates cell efficiency, FF, V_{oc} and I_{sc} of 5.34%, 61.8%, 205.5 mV, and 42.1 mA/cm^2, respectively. The investigation of P-i-N Ge cell and surface treatment on c-Ge using PH_3 exposure shows significant improvement of V_{oc} with better temperature coefficient [244,245]. Further studies are needed to improve the light absorption of Ge cell at thin absorber layer integrated with light-trapping techniques. It is worth noting that the high output power per unit area of TPV cells may offset the drawbacks related to their high cost, especially if the radiation temperature is high. For example, GaSb TPV under 1473 K radiation temperature reported an output power density of 0.82 W/cm^2, which was almost 30 times higher than the output generated from the best GaAs solar cell [181].

8.4. Low TPV Cell Conversion Efficiency

The low conversion efficiency of TPV cells remains the key challenge in realizing viable TPV system. The TPV cells efficiency losses can be categorized into two main factors, that are optical and electrical losses, as depicted in Figure 6. In particular, the losses associated with spectral mismatch and bandgap utilization were emphasized in Section 8.1.

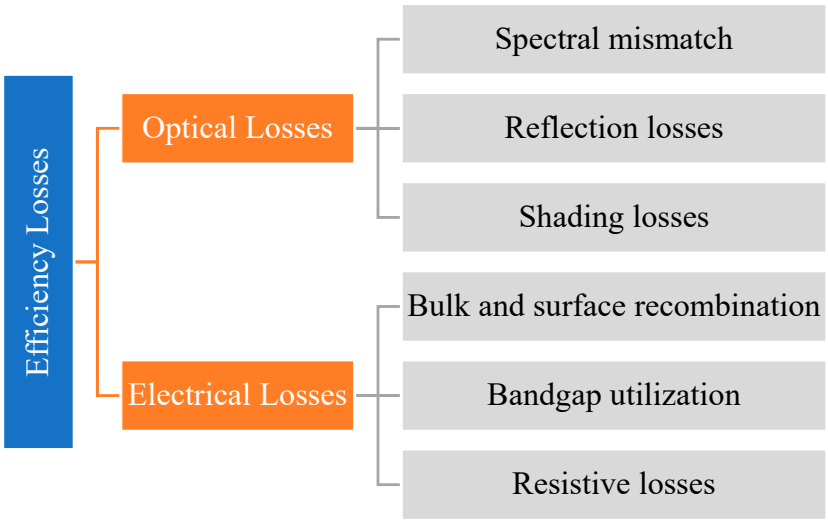

Figure 6. The TPV cells conversion efficiency losses.

The prediction of optical-to-electrical conversion efficiencies via fundamental calculation in TPV is comparable to solar PV technology. However, lower optical-to-electrical conversion efficiency of the overall TPV system is observed in the real condition [246]. This is mainly due to the poor spectral control from the generator up to the TPV cell, resulting in serious optical losses which are associated with the reflection and shading losses. The reflection problem can be mitigated by implementing an ARC as well as back surface reflector, while the shading loss can be reduced by optimizing the metal coverage area on the cell active surface.

Other than that, electrical losses such as bulk and surface recombination are the influencing factors of the cell conversion efficiency. For instance, majority of the reported works on InGaAs cell optimization focused on optimizing the electrical issue of the cell

and improving the V_{oc}. This was achieved by reducing the thickness of the absorber layer. However, the cell needs to be optically thick to absorb most of the incident illumination. Generally, TPV illumination flux is usually shifted to infrared wavelengths, and thicker absorber is needed to improve the absorption of infrared radiation and significantly increase J_{sc}. The use of intrinsic absorber layer in P-i-N or N-i-P TPV cells can increase J_{sc}, and increase the ratio of generation to recombination as the generated carriers in i-layer has high mobility and lifetime. Therefore, to maximize the cell efficiency, both optical and electrical losses must be considered to obtain an optimized designed TPV cell.

On the other hand, resistive losses are related to the effectiveness of the metal contact, which allows smooth transportation of the photogenerated carriers to the external circuit. Although the importance of metal contact is highly recognized, the study of ohmic contact to semiconductor materials received less attention. For example, the process technology for the fabrication and metallization techniques needs to be further developed to facilitate a good metal contact formation onto the GaSb semiconductor material. Other than that, the optimization of TPV cell ohmic superconductive metal contact would ease the flow of high current density. This can be achieved by designing transparent metamaterial metal with ohmic work function.

8.5. Near-Field TPV System

Near-field TPV system is designed by separating the radiator from the TPV cell by only a few nanometres to centimetres gap distance [11]. The amount of power transferred significantly decreases with longer travelling distance, that can be presented by the inverse square law [164]. In nanometer gap distance, there will be near-field coupling, resulting in Super-Planckian characteristic. In recent years, rapid developments in the theoretical, computational, and experimental investigation of near-field TPV have taken place due to its ability to increase the amount of energy transfer into TPV converter. The near-field TPV is still in the early stages of modeling and simulation, where different materials and techniques are being investigated. For example, the characterization of multi-layer graphene on the top of InSb TPV cell [247] and the optimization for near-field TPV using a genetic algorithm method [248]. Near-field TPV system performs much better than far-field system for gap distance between 12 μm to 60 nm under low-radiation temperature (<655 K) [249,250]. Near-field was also implemented in hybrid thermophotonic-PV and thermionic-PV converters. While the former uses light-emitting diode at the hot side to produce an output power of 9.6 W/cm^2 at 600 K radiator and 10 nm gap distance, the latter depends on both electrons and photons emission at the radiator [249,251]. Optimum near-field thermionic-PV converter has the potential to generate an output power density > 100 W/cm^2 at 2000 K radiation temperature [252].

9. Conclusions

Thermophotovoltaic system shows great benefits as an energy source with a full-time operating regime of blackbody temperature 500–2000 K as compared to solar photovoltaic system. The two dominant TPV technologies, which are the gallium antimonide and indium gallium arsenide, were extensively reviewed due to the vast integration in both industries and research areas. The fabrication of both cells is conducted based on non-epitaxial growth such as zinc diffusion and ion implantation methods, as well as epitaxial growth through liquid phase epitaxy, metal-organic vapor phase epitaxy and molecular beam epitaxy techniques. Non-epitaxial method is the preferable option as the manufacture can be done with low cost and less tedious procedures. On the other hand, an epitaxial of ternary of quaternary layer is essential to reduce the bandgap of the cell for a thermal photovoltaic system with heat source temperature of less than 1000 K. The performances for both cells were summarized in terms of several parameters such as open-circuit voltage, short-circuit current, current density and the cell efficiencies. In addition, the improvement for the cell performances was recapped with structural and functional optimization such

as metal contact, doping concentration, thickness, window, cap, buffer, surface field layers, graphene, metamaterial selective radiator and monolithic interconnected modules.

The practical applications for a thermal photovoltaic system include nuclear generator for space applications, hybrid electric vehicles, industrial and residential power supplies, waste heat recovery, solar thermophotovoltaic systems and portable electric generators. However, challenges in terms of spectral mismatching, internal cell temperature, and fabrication cost should be overcome to achieve a complete and more efficient thermophotovoltaic system. Hence, the key contribution of this study is the comprehensive analysis of gallium antimonide and indium gallium arsenide TPV cells to provide a tremendous outline on the improvement to the current achievement and their future deployment in the technology of energy and power system. The review has articulated some important and selective recommendations for the development of the TPV cells, and a few main research areas are listed below:

i. One of the main challenges that degrade the performance of TPV system is caused by the mismatch between the TPV spectral and the cell bandgap. Since optimum cell performance is achieved when the majority of the blackbody spectrum is absorbed in the TPV cell, it is crucial to select the suitable narrow bandgap material based on the heat source temperature. Furthermore, the efficient reflection and recycling of sub-bandgap photons in the radiator will significantly enhance the conversion efficiency of the TPV system.
ii. The cooling system in the TPV structure is significant since the cells are located near the heat radiator and exposed to the high radiant energy. Cell temperatures higher than 300 K lead to performance deterioration, and a cooling system should be considered to sustain the performance of the TPV system. The effective cooling system would consume the minimum energy and will play an important role to boost the future of TPV technology. The integration of PCM can help to cool the TPV system without any energy consumption. Furthermore, separating the cell from the radiator using transparent insulator or undoped semiconductor layer will help to reduce the cell temperature.
iii. The investigation to reduce the cost of TPV cells. The use of ELOG fabrication which sacrifice layer between the junction and the substrate which allows the integration of cheap substrates such as Si, GaAs and InP. Further development on the fabrication methods would significantly enhance the TPV cells performance with respect to their cost. It is worth noting that Ge semiconductor material has lower cost as compared to other narrow bandgap materials. However, the Ge TPV cell is required to be optically thick, and further studies on light trapping techniques are required to improve the light absorption of Ge cell at a thin absorber layer.
iv. The investigation of TPV cell conversion efficiency. TPV cells operate at high radiation energy, and the development of cell with minimum electrical and optical losses would significantly improve the output performance of TPV cells. Research on structures optimization for near-field TPV spectrums would help to reduce the optical and electrical losses in the semiconductor layers. Furthermore, the development of effective metal contact will significantly ease the flow of high current density. This can be achieved by engineering the ohmic superconductive/transparent metamaterial metal with ohmic work function. The transparent metal will cover the entire surface of the structure, which reduces the crowding effect with no impact to the light absorption in the absorber layer.
v. The development of the standard by which TPV cells are characterized, and the performances are determined. Previous reported works on TPV cells characterization vary in terms of the illumination intensity, the utilization of filter, and other measurement variations such as the variation of radiators, radiator temperature, cell temperatures, cavity geometry, and system scale, which makes the comparison of TPV cells a challenging task.

Author Contributions: M.M.A.G. wrote Sections 3, 5 and 8, H.J.L. contributed to writing Sections 1, 5 and 6, W.E.S.W.A.R. wrote Sections 4 and 7, P.J.K. wrote Section 9, L.K.Y. wrote Section 2, M.M.A.G., W.E.S.W.A.R., H.J.L. and P.J.K. revised the paper, P.J.K., M.A.H. and M.Z.J. supervised this project. All authors discussed and commented on the manuscript. All authors have read and agreed to the published version of the manuscript.

Funding: This research was funded by the Tenaga Nasional Berhad (TNB) seeding fund (Project code: U-TG-RD-18-04) managed by UNITEN R&D Sdn. Bhd. and the APC was funded by UNITEN Bold Refresh Publication Fund 2021, under Project J5100D4103.

Institutional Review Board Statement: Not applicable.

Informed Consent Statement: Not applicable.

Data Availability Statement: The data presented in this study are available on request from the corresponding author.

Conflicts of Interest: There are no conflict to declare.

Appendix A

Short Name	Full Name	Symbol	Unit	Meaning
TPV	Thermophotovoltaic	$P_{heat\ source}$	W/cm^2	Power of heating source
GaSb	Gallium antimonide	$P_{source\ loss}$	W/cm^2	Source heat loss
InGaAs	Indium gallium arsenide	$P_{radiant}$	W/cm^2	The radiant power
Ge	Germanium	P_{gap}	W/cm^2	The bandgap power
InAs	Indium arsenide	$P_{gap,loss}$	W/cm^2	The bandgap power loss
InGaAsSb	Indium gallium arsenide antimonide	$P_{recuperate}$	W/cm^2	The recuperated power
InAsSbP	Indium arsenide antimonide phosphide	P_{out}	W/cm^2	Output power
InGaAsSbP	Indium gallium arsenide antimonide phosphide	η	%	Cell efficiency
TE	Thermoelectric	P_{in}	W/cm^2	Input optical power
SiC	Silicon carbide	J_{sc}	A/cm^2	Short-circuit current density
W	Tungsten	V_{oc}	V	Open-circuit voltage
PhC	Photonics crystal	I_{sc}	A	Short-circuit current
YZA	Yttria-stabilised zirconia/alumina composite	FF	%	Fill factor
HEV	Hybrid electric vehicle	T_{cell}	K	Cell temperature
PCB	Pseudo-closed box	J_o	A/cm^2	Dark saturation current density
RTA	Rapid thermal annealing	n		Ideality factor
LPE	Liquid phase epitaxy	J_{ph}	A/cm^2	Photocurrent density
ELOG	Epitaxial lateral overgrowth	J	A/cm^2	Current density at the load
VPE	Vapour phase epitaxy	IV	AV	Current-voltage
MBE	Molecular beam epitaxy	e_o	coulomb	Charge
MOVPE	Metal-organic vapour phase epitaxy	J_m	A/cm^2	Maximum current density
PECVD	Plasma-enhanced chemical vapour deposition	V_m	V	Maximum voltage
Ni	Nickel	P_m	W/cm^2	Maximum power
Pd	Palladium	R_L	Ω	External load
Au	Gold	EQE	%	External quantum efficiency
Pt	Platinum	λ	m	Wavelength
Mo	Molybdenum	$\Phi(\lambda)$	m^{-2}s^{-1}	Incident photon flux
TCO	Transparent conductive oxide	$d(\lambda)$	m	Penetration distance
Si:H	Hydrogenated amorphous silicon interface	$R(\lambda)$	%	Reflection as a function of wavelength
MPhCs	Metallic photonic crystal	$P_{(x)}$	A/cm^2	Power received by the TPV cell
GaAs	Gallium arsenide	IQE	%	Internal quantum efficiency
InP	Indium phosphide	η_{TPV}	%	Efficiency of TPV system
NREL	National Renewable Energy Laboratory	η_{sp}	%	Spectral efficiency
SRH	Shockley-Read-Hall	$E(\lambda)$	W/cm^2. μm	Blackbody spectrum
MIMs	Monolithic Interconnected Modules	$\varepsilon(\lambda)$	n/a	Spectral emissivity
InGaSb	Indium gallium antimonide	E_g	eV	Bandgap energy
InSb	Indium antimonide	λ_c	m	Cut-off wavelength
InAsSb	Indium arsenide antimonide	λ_p	m	Peak emissivity
STPV	Solar TPV systems	n_i	cm^{-3}	Intrinsic concentration
CHP	Combined Heat and Power	QE	%	Quantum Efficiency
WHR	Waste Heat Recovery			
PCM	Phase change materials			
a-Si:H	Amorphous silicon			

References

1. Panayiotou, G.P.; Bianchi, G.; Georgiou, G.; Aresti, L.; Argyrou, M.; Agathokleous, R.; Tsamos, K.M.; Tassou, S.; Florides, G.; Kalogirou, S.; et al. Preliminary assessment of waste heat potential in major European industries. *Energy Procedia* **2017**, *123*, 335–345. [CrossRef]
2. Basu, S.; Chen, Y.-B.; Zhang, Z.M. Microscale radiation in thermophotovoltaic devices—A review. *Int. J. Energy Res.* **2007**, *31*, 689–716. [CrossRef]
3. Fraas, L.M. Economic potential for thermophotovoltaic electric power generation in the steel industry. In Proceedings of the 2014 IEEE 40th Photovoltaic Specialist Conference, PVSC 2014, Denver, CO, USA, 8–13 June 2014; pp. 766–770.
4. Bauer, T. *Thermophotovoltaics: Basic Principles and Critical Aspects of System Design*; Green Energy and Technology; Springer: Berlin/Heidelberg, Germany, 2011; Volume 7.
5. Rashid, W.E.; Gamel, M.M.A.; Ker, P.J.; Lau, K.Y.; Rahman, N.A.; Lee, H.J.; Jamaludin, M.Z. Optimization of zinc-doped emitter layer thickness and doping concentration for gallium antimonide based thermophotovoltaic cells. *ASM Sci. J.* **2019**, *12*, 1–9.
6. Licht, A.; Pfiester, N.; DeMeo, D.; Chivers, J.; Vandervelde, T. A Review of Advances in Thermophotovoltaics for Power Generation and Waste Heat Harvesting. *MRS Adv.* **2019**, *4*, 2271–2282. [CrossRef]
7. Ferrari, C.; Melino, F.; Pinelli, M.; Spina, P.R.; Venturini, M. Overview and Status of Thermophotovoltaic Systems. *Energy Procedia* **2014**, *45*, 160–169. [CrossRef]
8. Daneshvar, H.; Prinja, R.; Kherani, N.P. Thermophotovoltaics: Fundamentals, challenges and prospects. *Appl. Energy* **2015**, *159*, 560–575. [CrossRef]
9. Mustafa, K.F.; Abdullah, S.; Abdullah, M.; Sopian, K. A review of combustion-driven thermoelectric (TE) and thermophotovoltaic (TPV) power systems. Renew. Sustain. *Energy Rev.* **2017**, *71*, 572–584.
10. Datas, A.; Marti, A. Thermophotovoltaic energy in space applications: Review and future potential. *Sol. Energy Mater. Sol. Cells* **2017**, *161*, 285–296. [CrossRef]
11. Tian, Y.; Ghanekar, A.; Ricci, M.; Hyde, M.; Gregory, O.; Zheng, Y. A review of tunable wavelength selectivity of metamaterials in near-field and far-field radiative thermal transport. *Materials* **2018**, *11*, 862. [CrossRef] [PubMed]
12. Sakakibara, R.; Stelmakh, V.; Chan, W.R.; Ghebrebrhan, M.; Joannopoulos, J.D.; Soljačić, M.; Čelanović, I. Practical emitters for thermophotovoltaics: A review. *J. Photon Energy* **2019**, *9*, 032713. [CrossRef]
13. Rashid, W.E.S.W.A.; Ker, P.J.; Bin Jamaludin, Z.; Gamel, M.M.A.; Lee, H.J.; Rahman, N.B.A. Recent Development of Thermophotovoltaic System for Waste Heat Harvesting Application and Potential Implementation in Thermal Power Plant. *IEEE Access* **2020**, *8*, 105156–105168. [CrossRef]
14. Burger, T.; Sempere, C.; Roy-Layinde, B.; Lenert, A. Present Efficiencies and Future Opportunities in Thermophotovoltaics. *Joule* **2020**, *4*, 1660–1680. [CrossRef]
15. Utlu, Z.; Önal, B.S. Thermodynamic analysis of thermophotovoltaic systems used in waste heat recovery systems: An application. *Int. J. Low Carbon Technol.* **2018**, *13*, 52–60. [CrossRef]
16. Minotti, A. Energy Converter with Inside Two, Three, and Five Connected H2/Air Swirling Combustor Chambers: Solar and Combustion Mode Investigations. *Energies* **2016**, *9*, 461. [CrossRef]
17. Woolf, D.N.; Kadlec, E.A.; Bethke, D.; Grine, A.D.; Nogan, J.J.; Cederberg, J.G.; Burckel, D.B.; Luk, T.S.; Shaner, E.A.; Hensley, J.M. High-efficiency thermophotovoltaic energy conversion enabled by a metamaterial selective emitter. *Optica* **2018**, *5*, 213–218. [CrossRef]
18. Butcher, T.; Hammonds, J.; Horne, E.; Kamath, B.; Carpenter, J.; Woods, D. Heat transfer and thermophotovoltaic power generation in oil-fired heating systems. *Appl. Energy* **2011**, *88*, 1543–1548. [CrossRef]
19. Durisch, W.; Bitnar, B.; Von Roth, F.; Palfinger, G. Small thermophotovoltaic prototype systems. *Sol. Energy* **2003**, *75*, 11–15. [CrossRef]
20. Bitnar, B.; Durisch, W.; Mayor, J.C.; Sigg, H.; Tschudi, H.R. Characterisation of rare earth selective emitters for thermophotovoltaic applications. *Sol. Energy Mater. Sol. Cells* **2002**, *73*, 221–234. [CrossRef]
21. Fraas, L.; Ballantyne, R.; Hui, S.; Ye, S.-Z.; Gregory, S.; Keyes, J.; Avery, J.; Lamson, D.; Daniels, B. Commercial GaSb cell and circuit development for the Midnight Sun® TPV stove. *AIP Conf. Proc.* **1999**, *460*, 480–487.
22. Chen, Z.; Adair, P.L.; Rose, M.F. Investigation of energy conversion in TPV power generation prototype using blackbody/selective emitters. In Proceedings of the IECEC-97 Thirty-Second Intersociety Energy Conversion Engineering Conference (Cat. No.97CH6203), Honolulu, HI, USA, 27 July–1 August 1997; Volume 2, pp. 1097–1100.
23. Yang, W.M.; Chou, S.K.; Shu, C.; Li, Z.W.; Xue, H. A prototype microthermophotovoltaic power generator. *Appl. Phys. Lett.* **2004**, *84*, 3864–3866. [CrossRef]
24. Wenming, Y.; Siawkiang, C.; Chang, S.; Hong, X.; Zhiwang, L. Effect of wall thickness of micro-combustor on the performance of micro-thermophotovoltaic power generators. *Sens. Actuators A Phys.* **2005**, *119*, 441–445. [CrossRef]
25. Waitz, I.A.; Gauba, G.; Tzeng, Y.-S. Combustors for Micro-Gas Turbine Engines. *J. Fluids Eng.* **1998**, *120*, 109–117. [CrossRef]
26. Colangelo, G.; De Risi, A.; Laforgia, D. New approaches to the design of the combustion system for thermophotovoltaic applications. *Semicond. Sci. Technol.* **2003**, *18*, S262–S269. [CrossRef]
27. Colangelo, G.; De Risi, A.; Laforgia, D. Experimental study of a burner with high temperature heat recovery system for TPV applications. *Energy Convers. Manag.* **2006**, *47*, 1192–1206. [CrossRef]

28. Ghanekar, A.; Tian, Y.; Zhang, S.; Cui, Y.; Zheng, Y. Mie-metamaterials-based thermal emitter for near-field thermophotovoltaic systems. *Materials* **2017**, *10*, 885. [CrossRef]
29. Sakurai, A.; Matsuno, Y. Design and Fabrication of a Wavelength-Selective Near-Infrared Metasurface Emitter for a Thermophotovoltaic System. *Micromachines* **2019**, *10*, 157. [CrossRef]
30. Coutts, T.J. An overview of thermophotovoltaic generation of electricity. *Sol. Energy Mater. Sol. Cells* **2000**, *66*, 443–452. [CrossRef]
31. Sai, H.; Yugami, H. Thermophotovoltaic generation with selective radiators based on tungsten surface gratings. *Appl. Phys. Lett.* **2004**, *85*, 3399–3401. [CrossRef]
32. Iles, P.A.; Chu, C.L. Design and fabrication of thermophotovoltaic cells. In Proceedings of the 1994 IEEE 1st World Conference on Photovoltaic Energy Conversion—WCPEC (A Joint Conference of PVSC, PVSEC and PSEC), Waikoloa, HI, USA, 5–9 December 1994; Volume 2, pp. 1750–1753.
33. Rinnerbauer, V.; Lenert, A.; Bierman, D.M.; Yeng, Y.X.; Chan, W.R.; Geil, R.D.; Senkevich, J.J.; Joannopoulos, J.D.; Wang, E.N.; Soljačić, M.; et al. Metallic Photonic Crystal Absorber-Emitter for Efficient Spectral Control in High-Temperature Solar Thermophotovoltaics. *Adv. Energy Mater.* **2014**, *4*, 1400334. [CrossRef]
34. Nam, Y.; Yeng, Y.; Lenert, A.; Bermel, P.; Celanovic, I.; Soljačić, M.; Wang, E.N. Solar thermophotovoltaic energy conversion systems with two-dimensional tantalum photonic crystal absorbers and emitters. *Sol. Energy Mater. Sol. Cells* **2014**, *122*, 287–296. [CrossRef]
35. Coutts, T.J.; Wanlass, M.W.; Ward, J.S.; Johnson, S. A review of recent advances in thermophotovoltaics. In Proceedings of the Conference Record of the Twenty Fifth IEEE Photovoltaic Specialists Conference—1996, Washington, DC, USA, 13–17 May 1996; pp. 25–30.
36. Tobler, W.; Durisch, W. High-performance selective Er-doped YAG emitters for thermophotovoltaics. *Appl. Energy* **2008**, *85*, 483–493. [CrossRef]
37. Sai, H.; Yugami, H.; Nakamura, K.; Nakagawa, N.; Ohtsubo, H.; Maruyama, S. Selective Emission of $Al_2O_3/Er_3Al_5O_{12}$ Eutectic Composite for Thermophotovoltaic Generation of Electricity. *Jpn. J. Appl. Phys.* **2000**, *39*, 1957–1961. [CrossRef]
38. Ferrari, C.; Melino, F.; Pinelli, M.; Spina, P.R. Thermophotovoltaic energy conversion: Analytical aspects, prototypes and experiences. *Appl. Energy* **2014**, *113*, 1717–1730. [CrossRef]
39. Casady, J.; Johnson, R. Status of silicon carbide (SiC) as a wide-bandgap semiconductor for high-temperature applications: A review. *Solid State Electron.* **1996**, *39*, 1409–1422. [CrossRef]
40. Yang, W.; Chou, S.; Shu, C.; Li, Z.; Xue, H. Research on micro-thermophotovoltaic power generators. *Sol. Energy Mater. Sol. Cells* **2003**, *80*, 95–104. [CrossRef]
41. Wu, H.; Kaviany, M.; Kwon, O. Thermophotovoltaic power conversion using a superadiabatic radiant burner. *Appl. Energy* **2018**, *209*, 392–399. [CrossRef]
42. Gentillon, P.; Southcott, J.; Chan, S.; Taylor, R.A. Stable flame limits for optimal radiant performance of porous media reactors for thermophotovoltaic applications using packed beds of alumina. *Appl. Energy* **2018**, *229*, 736–744. [CrossRef]
43. Gentillon, P.; Singh, S.; Lakshman, S.; Zhang, Z.; Paduthol, A.; Ekins-Daukes, N.J.; Chan, Q.N.; Taylor, R.A. A comprehensive experimental characterisation of a novel porous media combustion-based thermophotovoltaic system with controlled emission. *Appl. Energy* **2019**, *254*, 113721. [CrossRef]
44. Chubb, L.; Flood, J.; Lowe, A. *High Efficiency Thermal to Electric Energy Conversion Using Selective Emitters and Spectrally Tuned Solar Cells*; National Aeronautics and Space Administration: Washington, DC, USA, 1992; Volume 105755.
45. Catchpole, K.; Lin, K.; Green, M.; Aberle, A.; Corkish, R.; Zhao, J.; Wang, A. Thin semiconducting layers and nanostructures as active and passive emitters for thermophotonics and thermophotovoltaics. Phys. E: Low-dimensional Syst. *Nanostructures* **2002**, *14*, 91–95.
46. Tong, J.K.; Hsu, W.C.; Huang, Y.; Boriskina, S.V.; Chen, G. Thin-film 'thermal well' emitters and absorbers for high-efficiency thermophotovoltaics. *Sci. Rep.* **2015**, *5*, 10661. [CrossRef] [PubMed]
47. Wernsman, B.; Siergiej, R.; Link, S.; Mahorter, R.; Palmisiano, M.; Wehrer, R.; Schultz, R.; Schmuck, G.; Messham, R.; Murray, S.; et al. Greater Than 20% Radiant Heat Conversion Efficiency of a Thermophotovoltaic Radiator/Module System Using Reflective Spectral Control. *IEEE Trans. Electron Devices* **2004**, *51*, 512–515. [CrossRef]
48. Maremi, H.H.C.; Tolessa, F.; Lee, N.; Choi, G.; Kim, T. Design of Multilayer Ring Emitter Based on Metamaterial for Thermophotovoltaic Applications. *Energies* **2018**, *11*, 2299. [CrossRef]
49. Tang, L.; Ye, H.; Xu, J. A novel zinc diffusion process for the fabrication of high-performance GaSb thermophotovoltaic cells. *Sol. Energy Mater. Sol. Cells* **2014**, *122*, 94–98. [CrossRef]
50. Tang, L.; Fraas, L.M.; Liu, Z.; Duan, H.; Xu, C. Doping Optimization in Zn-Diffused GaSb Thermophotovoltaic Cells to Increase the Quantum Efficiency in the Long Wave Range. *IEEE Trans. Electron Devices* **2017**, *64*, 5012–5018. [CrossRef]
51. Tang, L.; Fraas, L.M.; Liu, Z.; Xu, C.; Chen, X. Performance Improvement of the GaSb Thermophotovoltaic Cells With n-Type Emitters. *IEEE Trans. Electron Devices* **2015**, *62*, 2809–2815. [CrossRef]
52. Karlina, L.B.; Vlasov, A.S.; Kulagina, M.M.; Timoshina, N.K. Thermophotovoltaic cells based on In0.53Ga0.47As/InP heterostructures. *Semiconductors* **2006**, *40*, 346–350. [CrossRef]
53. Fraas, L.M.; Avery, J.E.; Gruenbaum, P.E.; Sundaram, V.S.; Emery, K.; Matson, R. Fundamental characterization studies of GaSb solar cells. In Proceedings of the Conference Record of the Twenty-Second IEEE Photovoltaic Specialists Conference-1991, Las Vegas, NV, USA, 7–11 October 1991; Volume 1, pp. 80–84.

54. Van der Heide, J. Thermophotovoltaics. *Compr. Renew. Energy* **2012**, *1*, 603–618.
55. Rahimi, N.; Aragon, A.A.; Shima, D.M.; Hains, C.; Busani, T.; Lavrova, O.; Balakrishnan, G.; Lester, L.F. Characterization of surface defects on Be-implanted GaSb. *J. Vac. Sci. Technol. B* **2014**, *32*, 04E109. [CrossRef]
56. Pearton, S.J.; Von Neida, A.R.; Brown, J.M.; Short, K.T.; Oster, L.J.; Chakrabarti, U.K. Ion implantation damage and annealing in InAs, GaSb, and GaP. *J. Appl. Phys.* **1988**, *64*, 629–636. [CrossRef]
57. Bhat, I.B.; Borrego, J.M.; Gutmann, R.J.; Ostrogorsky, A.G. TPV energy conversion: A review of material and cell related issues. In Proceedings of the Intersociety Energy Conversion Engineering Conference, Washington, DC, USA, 11–16 August 1996; Volume 2, pp. 968–973.
58. Vaughan, E.I.; Rahimi, N.; Balakrishnan, G.; Hecht, A.A. Thin-Film Gallium Antimonide for Room-Temperature Radiation Detection. *J. Electron. Mater.* **2015**, *44*, 3288–3293. [CrossRef]
59. Rahimi, N.; Herrera, D.J.; Abdallah, S.; Stelmakh, V.; Chan, W.R.; Celanovic, I.; Lester, L.F. Epitaxial and non-epitaxial large area GaSb-based thermophotovoltaic (TPV) cells. In Proceedings of the 2015 IEEE 42nd Photovoltaic Specialist Conference, PVSC 2015, New Orleans, LA, USA, 14–19 June 2015; pp. 2–4.
60. Rahimi, N.; Herrera, D.J.; Aragon, A.; Shima, D.M.; Romero, O.S.; Rotter, T.J.; Busani, T.; Lavrova, O.; Balakrishnan, G.; Lester, L.F. GaSb thermophotovoltaics: Current challenges and solutions. In Proceedings of the Physics, Simulation, and Photonic Engineering of Photovoltaic Devices IV. International Society for Optics and Photonics, San Francisco, CA, USA, 7 February 2015; p. 935816. [CrossRef]
61. Pearton, S.J. Ion implantation for isolation of III-V semiconductors. *Mater. Sci. Rep.* **1990**, *4*, 313–363. [CrossRef]
62. Tang, L.; Xu, C.; Liu, Z.; Lu, Q.; Marshall, A.; Krier, A. Suppression of the surface 'dead region' for fabrication of GaInAsSb thermophotovoltaic cells. *Sol. Energy Mater. Sol. Cells* **2017**, *163*, 263–269. [CrossRef]
63. Qiu, K.; Hayden, A.C.S. Direct thermal to electrical energy conversion using very low bandgap TPV cells in a gas-fired furnace system. *Energy Convers. Manag.* **2014**, *79*, 54–58. [CrossRef]
64. Herman, M.A.; Richter, W.; Sitter, H. *Epitaxy*; Springer: Berlin/Heidelberg, Germany, 2004; Volume 62.
65. Krier, A.; Yin, M.; Marshall, A.; Kesaria, M.; Krier, S.; McDougall, S.; Meredith, W.; Johnson, A.; Inskip, J.; Scholes, A. Low bandgap mid-infrared thermophotovoltaic arrays based on InAs. *Infrared Phys. Technol.* **2015**, *73*, 126–129. [CrossRef]
66. Mauk, M.G.; Tata, A.N.; Cox, J.A. Solution growth of thick III-V antimonide alloy epilayers (InAsSb, InGaSb, InGaAsSb, AlGaAsSb, and InAsSbP) for 'virtual substrates. *J. Cryst. Growth* **2001**, *225*, 236–243. [CrossRef]
67. Dobosz, D.; Zytkiewicz, Z.; Papis, E.; Kaminska, E.; Piotrowska, A. Epitaxial lateral overgrowth of GaSb layers by liquid phase epitaxy. *J. Cryst. Growth* **2003**, *253*, 102–106. [CrossRef]
68. Liu, Y.; Zytkiewicz, Z.; Dost, S. Computational analysis of lateral overgrowth of GaAs by liquid-phase epitaxy. *J. Cryst. Growth* **2005**, *275*, e953–e957. [CrossRef]
69. Cheetham, K.J.; Carrington, P.J.; Cook, N.B.; Krier, A. Solar Energy Materials & Solar Cells Low bandgap GaInAsSbP pentanary thermophotovoltaic diodes. *Sol. Energy Mater. Sol. Cells* **2011**, *95*, 534–537.
70. Gevorkyan, V.A.; Aroutiounian, V.M.; Gambaryan, K.M.; Kazaryan, M.S.; Touryan, K.J.; Wanlass, M.W. Liquid-phase electroepitaxial growth of low band-gap p-InAsPSb/n-InAs and p-InAsP/n-InAs diode heterostructures for thermo-photovoltaic application. *Thin Solid Film.* **2004**, *451*, 124–127. [CrossRef]
71. Biefeld, R.M. The metal-organic chemical vapor deposition and properties of III–V antimony-based semiconductor materials. *Mater. Sci. Eng. R Rep.* **2002**, *36*, 105–142. [CrossRef]
72. Mauk, M.G. Survey of Thermophotovoltaic (TPV) Devices. In *Mid-infrared Semiconductor Optoelectronics*; Springer: London, UK, 2006; Volume 118, pp. 673–738.
73. Cederberg, J.G.; Blaich, J.D.; Girard, G.R.; Lee, S.R.; Nelson, D.P.; Murray, C.S. The development of (InGa)As thermophotovoltaic cells on InP using strain-relaxed In(PAs) buffers. *J. Cryst. Growth* **2008**, *310*, 3453–3458. [CrossRef]
74. Wang, C.A. Correlation between surface step structure and phase separation in epitaxial GaInAsSb. *Appl. Phys. Lett.* **2000**, *76*, 2077–2079. [CrossRef]
75. Bouzid, F.; Dehimi, L. Performance evaluation of a GaSb thermophotovoltaic converter. *Rev. Energ. Renouvelables* **2012**, *15*, 3–383.
76. Schlegl, T. TPV Modules Based On GaSb Structures. *AIP Conf. Proc.* **2004**, *738*, 285–293.
77. Bumby, C.W.; Shields, P.A.; Nicholas, R.J.; Fan, Q.; Shmavonyan, G.; May, L.; Haywood, S.K. Improved Efficiency of GaSb/GaAs TPV Cells Using an Offset p-n Junction and Off-Axis (100) Substrates. In Proceedings of the Thermophotovoltaic Generation of Electricity: Sixth Conference on Thermophotovoltaic Generation of Electricity TPV6 (AIP Conference Proceedings), Freiberg, Germany, 15 December 2004; pp. 353–359.
78. Lu, Q.; Beanland, R.; Montesdeoca, D.; Carrington, P.J.; Marshall, A.; Krier, A. Low bandgap GaInAsSb thermophotovoltaic cells on GaAs substrate with advanced metamorphic buffer layer. *Sol. Energy Mater. Sol. Cells* **2019**, *191*, 406–412. [CrossRef]
79. Lu, Q.; Marshall, A.; Krier, A. Metamorphic integration of GaInAsSb material on GaAs substrates for light emitting device applications. *Materials* **2019**, *12*, 1743. [CrossRef] [PubMed]
80. Uppal, D.G.P.N.; Charache, G.; Baldasaro, P.; Campbell, B.; Loughin, S.; Svensson, S. MBE growth of GaInAsSb p/n junction diodes for thermophotovoltaic applications. *J. Cryst. Growth* **1997**, *176*, 877–882. [CrossRef]
81. Gozu, S.-I.; Mozume, T.; Kuwatsuka, H.; Ishikawa, H. Effects of shutter transients in molecular beam epitaxy. *Nanoscale Res. Lett.* **2012**, *7*, 620. [CrossRef] [PubMed]

82. Tournet, J.; Parola, S.; Vauthelin, A.; Cardenes, D.M.; Soresi, S.; Martinez, F.; Lu, Q.; Cuminal, Y.; Carrington, P.J.; Décobert, J.; et al. GaSb-based solar cells for multi-junction integration on Si substrates. *Sol. Energy Mater. Sol. Cells* **2019**, *191*, 444–450. [CrossRef]
83. Craig, A.P.; Thompson, M.D.; Tian, Z.-B.; Krishna, S.; Krier, A.; Marshall, A.R.J. InAsSb-based nBn photodetectors: Lattice mismatched growth on GaAs and low-frequency noise performance. *Semicond. Sci. Technol.* **2015**, *30*, 105011. [CrossRef]
84. Husain, S.B.; Hasan, M. Epitaxial Lattice Matching and the Growth Techniques of Compound Semiconductors for their Potential Photovoltaic Applications. *J. Mod. Mater.* **2017**, *5*, 34–42. [CrossRef]
85. Hudait, M.K.; Brenner, M.; Ringel, S.A. Metamorphic In0.7Al0.3As/In0.69Ga0.31As thermophotovoltaic devices grown on graded InAsyP1-y buffers by molecular beam epitaxy. *Solid. State. Electron.* **2009**, *53*, 102–106. [CrossRef]
86. Wang, C.A. Progress and continuing challenges in GaSb-based III-V alloys and heterostructures grown by organometallic vapor-phase epitaxy. *J. Cryst. Growth* **2004**, *272*, 664–681. [CrossRef]
87. Meharrar, F.Z.; Belfar, A.; Aouad, I.; Giudicelli, E.; Cuminal, Y.; Aït-kaci, H. Analysis of the GaSb-p+/GaSb-p/GaSb-n+/GaSb-n structure performances at room temperature, for thermo-photovoltaic applications. *Optik* **2018**, *175*, 138–147. [CrossRef]
88. Kasap, S.; Capper, P. *Springer Handbook of Electronic and Photonic Materials*; Springer International Publishing: Berlin/Heidelberg, Germany, 2017.
89. Moon, R.L. MOVPE: Is there any other technology for optoelectronics? *J. Cryst. Growth* **1997**, *170*, 1–10. [CrossRef]
90. Juang, B.-C.; Laghumavarapu, R.B.; Foggo, B.J.; Simmonds, P.J.; Lin, A.; Liang, B.; Huffaker, D.L. GaSb thermophotovoltaic cells grown on GaAs by molecular beam epitaxy using interfacial misfit arrays. *Appl. Phys. Lett.* **2015**, *106*, 111101. [CrossRef]
91. Hudait, M.K.; Lin, Y.; Palmisiano, M.N.; Ringel, S.A. 0.6-eV bandgap In0.69Ga0.31As thermophotovoltaic devices grown on InAsyP1-y step-graded buffers by molecular beam epitaxy. *IEEE Electron Device Lett.* **2003**, *24*, 538–540. [CrossRef]
92. Abdallah, S.A.; Herrera, D.J.; Conlon, B.P.; Rahimi, N.; Lester, L.F. Emitter thickness optimization for GaSb thermophotovoltaic cells grown by molecular beam epitaxy. In Proceedings of the Next Generation Technologies for Solar Energy Conversion VI, San Diego, CA, USA, 9 August 2015; Volume 9562, p. 95620L.
93. Wang, C.A.; Choi, H.K.; Turner, G.W.; Spears, D.L.; Manfra, M.J.; Charache, G.W. Lattice-matched epitaxial GaInAsSb/GaSb thermophotovoltaic devices. In Proceedings of the Third NREL Conference on thermophotovoltaic generation of electricity, New York, American Institute of Physics, Colorado Springs, CO, USA, May 1997; Volume 401, pp. 75–87. [CrossRef]
94. Fraas, L.M.; McLeod, P.S.; Partain, L.D.; Cape, J.A. GaSb films grown by vacuum chemical epitaxy using triethyl antimony and triethyl gallium sources. *J. Appl. Phys.* **1987**, *61*, 2861–2865. [CrossRef]
95. Mauk, M.G.; Andreev, V.M. GaSb-related materials for TPV cells. *Semicond. Sci. Technol.* **2003**, *18*, S191–S201. [CrossRef]
96. Welser, E.; Dimroth, F.; Ohm, A.; Guter, W.; Siefer, G.; Philipps, S.; Schöne, J.; Polychroniadis, E.K.; Konidaris, S.; Bett, A.W. Lattice-Matched GaInAsSb on GaSb for TPV Cells. *AIP Conf. Proc.* **2006**, *890*, 107–114.
97. Predan, F.; Ohlmann, J.; Mrabet, S.; Dimroth, F.; Lackner, D. Hall characterization of epitaxial GaSb and AlGaAsSb layers using p-n junctions on GaSb substrates. *J. Cryst. Growth* **2018**, *496*, 36–42. [CrossRef]
98. Sinharoy, S.; Weizer, V.G.; Wakchaure, Y.; Su, N.; Fay, P.; Scheiman, D. Development of a very high efficiency, dot-junction, InGaAs thermophotovoltaic (TPV) converter for deep space missions. In Proceedings of the Conference Record of the Thirty-first IEEE Photovoltaic Specialists Conference, Lake Buena Vista, FL, USA, 3–7 January 2005; pp. 766–769.
99. Dimroth, F.; Agert, C.; Bett, A.W. Growth of Sb-based materials by MOVPE. *J. Cryst. Growth* **2003**, *248*, 265–273. [CrossRef]
100. Shellenbarger, Z.A. High Performance InGaAsSb TPV Cells via Multi-Wafer OMVPE Growth. In Proceedings of the Thermophotovoltaic Generation of Electricity: Fifh NREL Conference, Rome, Italy, 6 February 2003; Volume 314, pp. 314–323.
101. Wilt, D.M.; Fatemi, N.S.; Hoffman, R.W.; Jenkins, P.P.; Brinker, D.J.; Scheiman, D.; Lowe, R.; Fauer, M.; Jain, R.K. High efficiency indium gallium arsenide photovoltaic devices for thermophotovoltaic power systems. *Appl. Phys. Lett.* **1994**, *64*, 2415–2417. [CrossRef]
102. Sodabanlu, H.; Watanabe, K.; Sugiyama, M.; Nakano, Y. Growth of InGaAs(P) in planetary metalorganic vapor phase epitaxy reactor using tertiarybutylarsine and tertiarybutylphosphine for photovoltaic applications. *Jpn. J. Appl. Phys.* **2018**, *57*, 08RD09. [CrossRef]
103. Kao, Y.-C.; Chou, H.-M.; Hsu, S.-C.; Lin, A.; Lin, C.-C.; Shih, Z.-H.; Chang, C.-L.; Hong, H.-F.; Horng, R.-H. Performance comparison of III–V//Si and III–V//InGaAs multi-junction solar cells fabricated by the combination of mechanical stacking and wire bonding. *Sci. Rep.* **2019**, *9*, 4308. [CrossRef]
104. Bumby, C.W.; Fan, Q.; Shields, P.A.; Nicholas, R.J.; Haywood, S.K.; May, L. InAs passivated GaSb thermo-photovoltaic cells on a GaAs substrate grown by MOVPE. *Int. J. Ambient Energy* **2004**, *25*, 73–78. [CrossRef]
105. Hitchcock, C.W.; Gutmann, R.J.; Borrego, J.M. Antimonide-based devices for thermophotovoltaic applications. *IEEE Trans. Electron Devices* **1999**, *46*, 2154–2161. [CrossRef]
106. Tournié, E.; Lazzari, J.L.; Pitard, F.; Alibert, C.; Joullié, A.; Lambert, B. 2.5 μm GaInAsSb lattice-matched to GaSb by liquid phase epitaxy. *J. Appl. Phys.* **1990**, *68*, 5936–5938. [CrossRef]
107. Mauk, M.; Shellenbarger, Z.; Cox, J.; Sulima, O.; Bett, A.; Mueller, R.; Sims, P.; McNeely, J.; DiNetta, L. Liquid-phase epitaxy of low-bandgap III–V antimonides for thermophotovoltaic devices. *J. Cryst. Growth* **2000**, *211*, 189–193. [CrossRef]
108. Shellenbarger, Z.A.; Mauk, M.G.; Cox, J.A.; Gottfried, M.I.; Sims, P.E.; Lesko, J.D.; McNeely, J.B.; DiNetta, L.C. Improvements in GaSb-based thermophotovoltaic cells. In Proceedings of the Third NREL Conference Thermophotovoltaic Generation of Electricity, New York, American Institute of Physics, Colorado Springs, CO, USA, May 1997; Volume 401, pp. 117–128. [CrossRef]

109. Shellenbarger, Z.A.; Mauk, M.G.; DiNetta, L.C.; Charache, G.W. Recent progress in InGaAsSb/GaSb TPV devices. In Proceedings of the Conference Record of the Twenty Fifth IEEE Photovoltaic Specialists Conference—1996, Washington, DC, USA, 13–17 May 1996; pp. 81–84.
110. Mani, H.; Tournié, E.; Lazzari, J.L.; Alibert, C.; Joullié, A.; Lambert, B. Liquid phase epitaxy and characterization of InAs1-x-ySb x P y on (100) InAs. *J. Cryst. Growth* **1992**, *121*, 463–472. [CrossRef]
111. Sundaram, V.S.; Saban, S.B.; Morgan, M.D.; Horne, W.E.; Evans, B.D.; Ketterl, J.R.; Morosini, M.B.Z.; Patel, N.B.; Field, H. GaSb based ternary and quaternary diffused junction devices for TPV applications. In Proceedings of the Third NREL Conference on thermophotovoltaic generation of electricity, New York, American Institute of Physics, Colorado Springs, CO, USA, May 1997; Volume 105, pp. 105–115. [CrossRef]
112. Ye, H.; Tang, L.; Li, K. The intrinsic relationship between the kink-and-tail and box-shaped zinc diffusion profiles in n-GaSb. *Semicond. Sci. Technol.* **2013**, *28*, 015001. [CrossRef]
113. Bett, A.W.; Sulima, O.V. GaSb photovoltaic cells for applications in TPV generators. *Semicond. Sci. Technol.* **2003**, *18*, S184–S190. [CrossRef]
114. Khvostikov, V.P.; Khvostikova, O.A.; Gazaryan, P.Y.; Sorokina, S.V.; Potapovich, N.S.; Malevskaya, A.V.; Kaluzhniy, N.A.; Shvarts, M.Z.; Andreev, V.M. Photovoltaic Cells Based on GaSb and Ge for Solar and Thermophotovoltaic Applications. *J. Sol. Energy Eng.* **2006**, *129*, 291–297. [CrossRef]
115. Akano, U.G.; Mitchell, I.V.; Shepherd, F.R.; Miner, C.J. Ion implantation damage of InP and InGaAs. *Nucl. Inst. Methods Phys. Res. B* **1995**, *106*, 308–312. [CrossRef]
116. Gerber, A.H. Arc Chamber for an ion implantation system. U.S. Patent 5857889A, 27 March 1996.
117. Ni, Q.; Ye, H.; Shu, Y.; Lin, Q. A theoretical discussion on the internal quantum efficiencies of the epitaxial single crystal GaSb thin film cells with different p–n junctions. *Sol. Energy Mater. Sol. Cells* **2016**, *149*, 88–96. [CrossRef]
118. Ferguson, L.G.; Fraas, L.M. Theoretical study of GaSb PV cells efficiency as a function of temperature. *Sol. Energy Mater. Sol. Cells* **1995**, *39*, 11–18. [CrossRef]
119. Lewis Fraas, E.M.L.; Veeravana, S.; James, A.; Peter, G. III-V Solar Cells And Doping Processing. U.S. Patent 5,217,539, 8 June 1993.
120. Fraas, L.M.; Avery, J.E.; Huang, H.X. Thermophotovoltaics: Heat and electric power from low bandgap "solar" cells around gas fired radiant tube burners. In Proceedings of the Conference Record of the Twenty-Ninth IEEE Photovoltaic Specialists Conference, 2002, New Orleans, LA, USA, 19–24 May 2002; Volume 1, pp. 1553–1556.
121. Fraas, L.; Ballantyne, R.; Samaras, J.; Seal, M. Electric power production using new GaSb photovoltaic cells with extended infrared response. *AIP Conf. Proc.* **1994**, *321*, 44–53.
122. Seal, M.; Christ, S.; Campbell, G.; West, E.; Fraas, L. Thermophotovoltaic generation of power for use in a series hybrid vehicle. *SAE Tech. Pap.* **1997**. [CrossRef]
123. Morrison, O.; Seal, M.; West, E.; Connelly, W. Use of a thermophotovoltaic generator in a hybrid electric vehicle. In Proceedings of the Thermophotovoltaic Generation of Electricity, Fourth NREL Conference AIP Conference Proceeding, Denver, CO, USA, 11–14 October 1998; Volume 460, pp. 488–496.
124. Stollwerck, G.; Sulima, O.; Bett, A. Characterization and simulation of GaSb device-related properties. *IEEE Trans. Electron. Devices* **2000**, *47*, 448–457. [CrossRef]
125. Utlu, Z. Investigation of the potential for heat recovery at low, medium, and high stages in the Turkish industrial sector (TIS): An application. *Energy* **2015**, *81*, 394–405. [CrossRef]
126. Utlu, Z.; Paralı, U.; Gültekin, C. Applicability of Thermophotovoltaic Technologies in the Iron and Steel Sectors. *Energy Technol.* **2018**, *6*, 1039–1051. [CrossRef]
127. Utlu, Z.; Önal, B.S. Performance evaluation of thermophotovoltaic GaSb cell technology in high temperature waste heat. *IOP Conf. Ser. Mater. Sci. Eng.* **2018**, *307*, 012075. [CrossRef]
128. McLeod, P.S.; Cape, J.A.; Fraas, L.M.; Partain, L.D. GaAs on GaSb Mechanically Stacked Photovoltaic Cells, Package Assembly, and Modules. U.S. Patent 776,893, 11 October 1988.
129. Fraas, L.M.; Mansoori, N.; Avery, J.E.; Martin, J.M.; Yerkes, J.W. Panel For Solar Concentrators and Tandem Cell Units. U.S. Patent 5096505, 17 March 1992.
130. Fraas, L.M.; Avery, J.E.; Girard, G.R. Tandem Photovoltaic Solar Cell With III-V Diffused Junction Booster Cell. U.S. Patent 5123968, 19 June 1991.
131. Fraas, L.M.; E Avery, J.; Huang, H.X. Thermophotovoltaic furnace–generator for the home using low bandgap GaSb cells. *Semicond. Sci. Technol.* **2003**, *18*, S247–S253. [CrossRef]
132. Martín, D. Theoretical Comparison between Diffused and Epitaxial GaSb TPV Cells. In Proceedings of the AIP Conference Proceedings 738; TPV6: Sixth World Conference on Thermophotovoltaic Generation of Electricity, Freiburg, Germany, 7 December 2004; Volume 738, pp. 311–319.
133. Khvostikov, V.P.; Gazaryan, P.Y.; Khvostikova, O.A.; Potapovich, N.S.; Sorokina, S.V.; Malevskaya, A.V.; Shvarts, M.Z.; Shmidt, N.M.; Andreev, V.M. GaSb Applications for Solar Thermophotovoltaic Conversion. In Proceedings of the Thermophotovoltaic Generation of Electricity: Seventh World Conference on Thermophotovoltaic Generation of Electricity (AIP Conference Proceedings), Madrid, Spain, 9 March 2007; Volume 890, pp. 139–148.
134. Khvostikov, V.P.; Sorokina, S.V.; Potapovich, N.S.; Khvostikova, O.A.; Malievskaya, A.V.; Vlasov, A.; Shvarts, M.; Timoshina, N.K.; Andreev, V.M. Thermophotovoltaic generators based on gallium antimonide. *Semiconductors* **2010**, *44*, 255–262. [CrossRef]

135. Wu, X.; Ye, H.; Wang, J. Experimental analysis of cell output performance for a TPV system. *Sol. Energy Mater. Sol. Cells* **2011**, *95*, 2459–2465. [CrossRef]
136. Fraas, L.M.; Tang, L.; Zhang, Y. Designing a Heterojunction N+ on P GaSb Thermophotovoltaic Cell with hydrogenated Amorphous Silicon Interface Passivation. In Proceedings of the 2018 IEEE 7th World Conference on Photovoltaic Energy Conversion (WCPEC) (A Joint Conference of 45th IEEE PVSC, 28th PVSEC & 34th EU PVSEC), Waikoloa, HI, USA, 10–15 June 2018; pp. 0887–0890.
137. Fraas, L.; Minkin, L.; Avery, J.; Ferguson, L.; Samaras, J. Spectral control development for Thermophotovoltaics. In Proceedings of the 2016 IEEE 43rd Photovoltaic Specialists Conference (PVSC), Portland, OR, USA, 5–10 June 2016; pp. 1–5.
138. Rahimi, N.; Aragon, A.A.; Romero, O.S.; Shima, D.M.; Rotter, T.J.; Balakrishnan, G.; Mukherjee, S.D.; Lester, L.F. Ultra-low resistance NiGeAu and PdGeAu ohmic contacts on N-GaSb grown on GaAs. In Proceedings of the 2013 IEEE 39th Photovoltaic Specialists Conference, Tampa, FL, USA, 16–21 June 2013; pp. 2123–2126.
139. Rahimi, N.; Aragon, A.A.; Romero, O.S.; Kim, D.M.; Traynor, N.B.J.; Rotter, T.J.; Balakrishnan, G.; Mukherjee, S.D.; Lester, L.F. Ohmic contacts to n-type GaSb grown on GaAs by the interfacial misfit dislocation technique. *Phys. Simul. Photonic Eng. Photovolt. Devices II* **2013**, *8620*, 86201K.
140. Rahimi, N.; Aragon, A.A.; Romero, O.S.; Kim, D.M.; Traynor, N.B.J.; Rotter, T.J.; Balakrishnan, G.; Mukherjee, S.D.; Lester, L.F. Electrical and microstructure analysis of nickel-based low-resistance ohmic contacts to n-GaSb. *APL Mater.* **2013**, *1*, 062105. [CrossRef]
141. Rahimi, N.; Aragon, A.A.; Romero, O.S.; Kim, D.M.; Traynor, N.B.J.; Rotter, T.J.; Balakrishnan, G.; Mukherjee, S.D.; Lester, L.F. Low resistance palladium/molybdenum based ohmic contacts to n-GaSb grown on GaAs. *J. Vac. Sci. Technol. B Nanotechnol. Microelectron. Mater. Process. Meas. Phenom.* **2014**, *32*, 04E108. [CrossRef]
142. Herrera, D.J.; Rahini, N.; Conlon, B.; Barbieri, P.; Barker, C.; Erb, D.; Park, C.; Abdallah, S.; Lester, L.F. Impact of the front metal layout on the fill factor of GaSb-based photovoltaics grown on n-type substrate. In Proceedings of the 2015 IEEE Photonics Conference IPC 2015, Reston, VA, USA, 4–8 October 2015; Volume 5, pp. 525–526.
143. Lou, Y.-Y.; Zhang, X.-L.; Huang, A.-B.; Wang, Y. Enhanced thermal radiation conversion in a GaSb/GaInAsSb tandem thermophotovoltaic cell. *Sol. Energy Mater. Sol. Cells* **2017**, *172*, 124–132. [CrossRef]
144. Wang, Y.; Zhang, X.; Zhang, X.; Chen, N. Electricity generation from thermal irradiation governed by GaSb active layer. *Renew. Energy* **2012**, *48*, 231–237. [CrossRef]
145. Milnes, A.; Polyakov, A. Gallium antimonide device related properties. *Solid-State Electron.* **1993**, *36*, 803–818. [CrossRef]
146. Milnes, A.G.; Ye, M.; Stam, M. Ohmic Contacts of Au and Ag to p-GaSb. *Solid State Electron.* **1994**, *37*, 37–44. [CrossRef]
147. Huang, R.K.; Wang, C.A.; Harris, C.T.; Connors, M.K.; Shiau, D.A. Ohmic contacts to n-type GaSb and n-type GaInAsSb. *J. Electron. Mater.* **2004**, *33*, 1406–1410. [CrossRef]
148. Sulima, O.; Bett, A. Fabrication and simulation of GaSb thermophotovoltaic cells. *Sol. Energy Mater. Sol. Cells* **2001**, *66*, 533–540. [CrossRef]
149. Rajagopalan, G.; Reddy, N.; Ehsani, E.; Bhat, I.; Dutta, P.; Gutmann, R.; Nichols, G.; Charache, G.; Sulima, O. A simple single-step diffusion and emitter etching process for high-efficiency gallium-antimonide thermophotovoltaic devices. *J. Electron. Mater.* **2003**, *32*, 1317–1321. [CrossRef]
150. Bett, A.W.; Keser, S.; Stollwerck, G.; Sulima, O.V.; Wettling, W. GaSb-based (thermo)photovoltaic cells with Zn diffused emitters. In Proceedings of the Conference Record of the Twenty Fifth IEEE Photovoltaic Specialists Conference—1996, Washington, DC, USA, 13–17 May 1996.
151. Licht, A.S.; Shemelya, C.S.; DeMeo, D.F.; Carlson, E.S.; Vandervelde, T. Optimization of GaSb thermophotovoltaic diodes with metallic photonic crystal front-surface filters. In Proceedings of the 2017 IEEE 60th International Midwest Symposium on Circuits and Systems (MWSCAS), Boston, MA, USA, 6–9 August 2017; pp. 843–846.
152. Tang, L.; Fraas, L.M.; Liu, Z.; Zhang, Y.; Duan, H.; Xu, C. N-type vapor diffusion for the fabrication of GaSb thermophotovoltaic cells to increase the quantum efficiency in the long wavelength range. *Sol. Energy Mater. Sol. Cells* **2019**, *194*, 137–141. [CrossRef]
153. Ma, D.; Deng, Y.; Wang, D.; Ji, W.; Li, E. Photoelectric properties of InxGa1-xAs: A first-principles study. *Superlattices Microstruct.* **2019**, *128*, 312–318. [CrossRef]
154. Matsubara, H.; Tanabe, T.; Moto, A.; Mine, Y.; Takagishi, S. Over 27% efficiency GaAs/InGaAs mechanically stacked solar cell. *Sol. Energy Mater. Sol. Cells* **1998**, *50*, 177–184. [CrossRef]
155. Tan, M.; Lu, S.; Ji, L.; Zhu, Y.; Chen, Z. Optimization of In0.68Ga0.32As thermophotovoltaic device grown on compositionally nonmonotonically graded InAsP buffer by metal-organic chemical vapor deposition. *Jpn. J. Appl. Phys.* **2013**, *52*, 116504. [CrossRef]
156. Ji, L.; Lu, S.; Jiang, D.; Zhao, Y.; Tan, M.; Zhu, Y.; Dong, J. 0.6-eV bandgap In0.69Ga0.31As thermophotovoltaic devices with compositionally undulating step-graded InAsyP1-ybuffers. *Chin. Phys. B* **2013**, *22*, 026802. [CrossRef]
157. Li, M.; Lee, J.; Oh, J.; Lee, H.D. Tb/Ni/TiN Stack for Ultralow Contact Resistive Ni-Tb-InGaAs Alloy to n-In0.53Ga0.47As Layer. *Phys. Status Solidi Rapid Res. Lett.* **2018**, *12*, 10–13. [CrossRef]
158. Tuley, R.S.; Nicholas, R.J. Material parameters and device optimization: Supplementary information for bandgap dependent thermophotovoltaic device performance using the InGaAs and InGaAsP material system. *J. Appl. Phys.* **2010**, *108*, 156018. [CrossRef]

159. Tan, M.; Ji, L.; Wu, Y.; Dai, P.; Wang, Q.; Li, K.; Yu, T.; Yu, Y.; Lu, S.; Yang, H. Investigation of InGaAs thermophotovoltaic cells under blackbody radiation. *Appl. Phys. Express* **2014**, *7*, 096601. [CrossRef]
160. Green, M.A.; Hishikawa, Y.; Dunlop, E.D.; Levi, D.H.; Hohl-Ebinger, J.; Ho-Baillie, A.W.Y. Solar cell efficiency tables (version 52). *Prog. Photovolt. Res. Appl.* **2018**, *26*, 427–436. [CrossRef]
161. Wanlass, M.W.; Carapella, J.J.; Duda, A.; Emery, K.; Gedvilas, L.; Moriarty, T.; Ward, S.; Webb, J.D.; Wu, X.; Murray, C.S. High-performance, 0.6-eV, $Ga_{0.32}In_{0.68}As/InAs_{0.32}P_{0.68}$ thermophotovoltaic converters and monolithically interconnected modules. *AIP Conf. Proc.* **1999**, *460*, 132–141.
162. Zhou, T.; Sun, Z.; Li, S.; Liu, H.; Yi, D. Design and Optimization of Thermophotovoltaic System Cavity with Mirrors. *Energies* **2016**, *9*, 722. [CrossRef]
163. Wojtczuk, S. Low bandgap InGaAs thermophotovoltaic cells. In Proceedings of the IECEC 96 31st Intersociety Energy Conversion Engineering Conference, Washington, DC, USA, 11–16 August 1996; Volume 2, pp. 974–978.
164. Tuley, R.S.; Orr, J.M.S.; Nicholas, R.; Rogers, D.C.; Cannard, P.J.; Dosanjh, S. Lattice-matched InGaAs on InP thermophovoltaic cells. *Semicond. Sci. Technol.* **2012**, *28*, 015013. [CrossRef]
165. Gamel, M.M.A.; Ker, P.J.; Rashid, W.E.S.W.A.; Lee, H.J.; Hannan, M.A.; Bin Jamaludin, Z. Performance of Ge and In0.53Ga0.47 as Thermophotovoltaic Cells under Different Spectral Irradiances. *IEEE Access* **2021**, *9*, 37091–37102. [CrossRef]
166. Su, N.; Fay, P.; Sinharoy, S.; Forbes, D.; Scheiman, D. Characterization and modeling of InGaAs/InAsP thermophotovoltaic converters under high illumination intensities. *J. Appl. Phys.* **2007**, *101*, 064511. [CrossRef]
167. Zhang, Z.; Miao, G.; Song, H.; Li, D.; Jiang, H.; Li, Z.; Chen, Y.; Sun, X. High in content InGaAs near-infrared detectors: Growth, structural design and photovoltaic properties. *Appl. Phys. A Mater. Sci. Process.* **2017**, *123*, 219. [CrossRef]
168. Zhao, L.; Guo, Z.; Ding, X.; Li, J.; Yang, S.; Zhang, M.; Zhao, L. Effects of $In_{0.82}Ga_{0.18}As/InP$ double buffers design on the microstructure of the $In_{0.82}G_{0.18}As/Inp$ heterostructure. *Crystals* **2017**, *7*, 155. [CrossRef]
169. Zhang, M.; Guo, Z.; Zhao, L.; Yang, S.; Zhao, L. The Effect of Buffer Types on the $In_{0.82}Ga_{0.18}As$ Epitaxial Layer Grown on an InP (100) Substrate. *Materials* **2018**, *11*, 975. [CrossRef] [PubMed]
170. Emziane, M.; Nicholas, R.J. Optimization of InGaAs(P) photovoltaic cells lattice matched to InP. *Am. Inst. Phys.* **2007**, *101*, 054503. [CrossRef]
171. Emziane, M.; Nicholas, R.J.; Rogers, D.C.; Cannard, P.J. Fabrication and Assessment of Optimized InGaAs Single-Junction TPV Cells. *AIP Conf. Proc.* **2007**, *890*, 149–156.
172. Nishikawa, W.; Joslin, D.; Krut, D.; Eldredge, J.; Narayanan, A.; Takahashi, M.; Haddad, H.; Al-Jassim, M.M.; Karam, N.H. Fabrication and electrical characterization of 0.55eV N-on-P InGaAs TPV devices. *AIP Conf. Proc.* **1999**, *427*, 427–437. [CrossRef]
173. Wojtczuk, S. Comparison of 0.55eV InGaAs single-junction vs. multi-junction TPV technology. In Proceedings of the Third NREL Conference on thermophotovoltaic generation of electricity, New York, American Institute of Physics, Colorado Springs, CO, USA, May 1997; Volume 205, pp. 205–213. [CrossRef]
174. Wojtczuk, S.; Colter, P.; Charache, G.; DePoy, D. Performance status of 0.55eV InGaAs thermophotovoltaic cells. In Proceedings of the Thermophotovoltaic Generation of Electricity: Fourth NREL Conference, Denver, CO, USA, 1 April 1999; Volume 417, pp. 417–426. [CrossRef]
175. Wehrer, R.J. 0.52 eV InGaAs/InPAs Thermophotovoltaic Cells. *AIP Conf. Proc.* **2004**, *738*, 445–452.
176. Wojtczuk, S.; Gagnon, E.; Geoffroy, L.; Parodos, T. InxGa1−xAs thermophotovoltaic cell performance vs. bandgap. *AIP Conf. Proc.* **1995**, *321*, 177–187.
177. Zhang, Y.; Gu, Y.; Zhu, C.; Hao, G.; Li, A.; Liu, T. Gas source MBE grown wavelength extended 2.2 and 2.5 μm InGaAs PIN photodetectors. *Infrared Phys. Technol.* **2006**, *47*, 257–262. [CrossRef]
178. Shi, Y.-H.; Zhang, Y.-G.; Ma, Y.-J.; Gu, Y.; Chen, X.-Y.; Gong, Q.; Du, B.; Zhang, J.; Zhu, Y. Improved performance of In0.83Ga0.17As/InP photodetectors through modifying the position of In0.66Ga0.34As/InAs superlattice electron barrier. *Infrared Phys. Technol.* **2018**, *89*, 72–76. [CrossRef]
179. Arslan, Y.; Oguz, F.; Besikci, C. Extended wavelength SWIR InGaAs focal plane array: Characteristics and limitations. *Infrared Phys. Technol.* **2015**, *70*, 134–137. [CrossRef]
180. Baraskar, A.K.; Wistey, M.A.; Lee, Y.J.; Gossard, A.C.; Rodwell, M.J.W. Ultralow resistance, nonalloyed Ohmic contacts to n-InGaAs. *J. Vac. Sci. Technol. B Microelectron. Nanom. Struct.* **2009**, *27*, 2036. [CrossRef]
181. Gamel, M.M.A.; Ker, P.J.; Lee, H.J.; Rashid, W.E.S.W.A.; Hannan, M.A.; David, J.P.R.; Jamaludin, M.Z. Multi-dimensional optimization of In0.53Ga0.47As thermophotovoltaic cell using real coded genetic algorithm. *Sci. Rep.* **2021**, *11*, 7741. [CrossRef] [PubMed]
182. Jain, R.K. Indium Phosphide Window Layers For Indium Gallium Arsenide Solar Cells. In Proceedings of the 18th Space Photovoltaic Research Technology Conference NASA/CP, Cleveland, OH, USA, 16–18 September 2003; pp. 126–133.
183. Mertens, K. Structure and Method of Operation of Solar Cells. In *Photovoltaics: Fundamentals, Technology and Practice*; John Wiley & Sons: Chichester, UK, 2014.
184. Jurczak, P.; Onno, A.; Sablon, K.; Liu, H. Efficiency of GaInAs thermophotovoltaic cells: The effects of incident radiation, light trapping and recombinations. *Opt. Express* **2015**, *23*, A1208. [CrossRef] [PubMed]
185. Fan, D.; Burger, T.; McSherry, S.; Lee, B.; Lenert, A.; Forrest, S.R. Near-perfect photon utilization in an air-bridge thermophotovoltaic cell. *Nature* **2020**, *586*, 237–241. [CrossRef] [PubMed]

186. Omair, Z.; Scranton, G.; Pazos-Outón, L.M.; Xiao, T.P.; Steiner, M.A.; Ganapati, V.; Peterson, P.F.; Holzrichter, J.; Atwater, H.; Yablonovitch, E. Ultraefficient thermophotovoltaic power conversion by band-edge spectral filtering. *Proc. Natl. Acad. Sci. USA* **2019**, *116*, 15356–15361. [CrossRef]
187. Wilt, D.M.; Fatemi, N.S.; Jenkins, P.P.; Hoffman, R.W.; Landis, G.A.; Jain, R.K. Monolithically interconnected InGaAs TPV module development. In Proceedings of the Conference Record of the Twenty Fifth IEEE Photovoltaic Specialists Conference—1996, Washington, DC, USA, 13–17 May 1996; pp. 43–48.
188. Datas, A.; Linares, P. Monolithic interconnected modules (MIM) for high irradiance photovoltaic energy conversion: A comprehensive review. *Renew. Sustain. Energy Rev.* **2017**, *73*, 477–495. [CrossRef]
189. Charache, G.W.; Depoy, D.M.; Baldasaro, P.F.; Campbell, B.C. Thermophotovoltaic devices utilizing a back surface reflector for spectral control. *AIP Conf. Proc.* **1996**, *358*, 339–350.
190. Wehrer, R.; Wanlass, M.; Wilt, D.; Wernsman, B.; Siergiej, R.; Carapella, J. InGaAs series-connected, tandem, MIM TPV converters. In Proceedings of the 3rd World Conference on Photovoltaic Energy Conversion, Osaka, Japan, 11–18 May 2003; Volume 1, pp. 892–895.
191. Woolf, D.; Hensley, J.; Cederberg, J.G.; Bethke, D.T.; Grine, A.D.; Shaner, E.A. Heterogeneous metasurface for high temperature selective emission. *Appl. Phys. Lett.* **2014**, *105*, 081110. [CrossRef]
192. Gamel, M.M.A.; Ker, P.J.; Lee, H.J.; Rashid, W.E.S.W.A.; Jamaludin, M.Z.; Mohammed, A.I.A. Performance Comparison of Narrow Bandgap Semiconductor Cells for Photovoltaic and Thermophotovoltaic Application. In Proceedings of the 2020 IEEE 8th International Conference on Photonics (ICP), Kota Bharu, Malaysia, 12 May–30 June 2020.
193. Sulima, O.V.; Bett, A.W.; Dutta, P.S.; Mauk, M.G.; Mueller, R.L. GaSb-, InGaAsSb-, InGaSb-, InAsSbP- and Ge-TPV cells with diffused emitters. In Proceedings of the Conference Record of the Twenty-Ninth IEEE Photovoltaic Specialists Conference, New Orleans, LA, USA, 19–24 May 2002; pp. 892–895.
194. Bitnar, B. Silicon, germanium and silicon/germanium photocells for thermophotovoltaics applications. *Semicond. Sci. Technol.* **2003**, *18*, S221–S227. [CrossRef]
195. Gamel, M.M.A.; Jern, K.P.; Rashid, W.E.; Yau, L.K.; Jamaludin, M.Z. The Effect of Illumination Intensity on the Performance of Germanium Based-Thermophotovoltaic Cell. In Proceedings of the 2019 IEEE Regional Symposium on Micro and Nanoelectronics (RSM), Pahang, Malaysia, 21–23 August 2019; pp. 129–132.
196. Sansoni, P.; Fontani, D.; Francini, F.; Jafrancesco, D.; Gabetta, G.; Casale, M.; Campesato, R.; Toniato, G. Evaluation of elliptical optical cavity for a combustion thermophotovoltaic system. *Sol. Energy Mater. Sol. Cells* **2017**, *171*, 282–292. [CrossRef]
197. Penumaka, R.; Tiwari, B.; Bhattacharya, I.; Foo, S. Indium Gallium Antimonide a better bottom subcell layer in III–V multijunction solar cells. In Proceedings of the 2015 IEEE 42nd Photovoltaic Specialist Conference (PVSC), New Orleans, LA, USA, 14–19 June 2015; pp. 1–5.
198. Wang, Y.; Lou, Y.Y. Radiant thermal conversion in 0.53eV GaInAsSb thermophotovoltaic diode. *Renew. Energy* **2015**, *75*, 8–13. [CrossRef]
199. Tang, L.; Fraas, L.M.; Liu, Z.; Xu, C.; Chen, X. The Theoretical Performance of GaInAsSb and GaSb Cells Versus IR Emitter Temperature in Thermophotovoltaic Systems. *IEEE Trans. Electron Devices* **2016**, *63*, 3591–3598. [CrossRef]
200. Peng, X.; Liu, Y.; Zou, J.; Deng, W. An Analysis on Device-related Properties of the GaInSb Thermophotovoltaic Cell. *DEStech Trans. Environ. Energy Earth Sci.* **2018**, 336–344. [CrossRef]
201. Lotfi, H.; Li, L.; Lei, L.; Yang, R.Q.; Klem, J.F.; Johnson, M.B. Narrow-Bandgap Interband Cascade Thermophotovoltaic Cells. *IEEE J. Photovoltaics* **2017**, *7*, 1462–1468. [CrossRef]
202. Sulima, O.V.; Bett, A.W.; Mauk, M.G.; Dimroth, F.; Dutta, P.S.; Mueller, R.L. GaSb-, InGaAsSb-, InGaSb-, InAsSbP- and Ge-TPV cells for low-temperature TPV applications. *AIP Conf. Proc.* **2003**, *653*, 434.
203. Lu, Q.; Zhou, X.; Krysa, A.; Marshall, A.; Carrington, P.; Tan, C.-H.; Krier, T. InAs thermophotovoltaic cells with high quantum efficiency for waste heat recovery applications below 1000 °C. *Sol. Energy Mater. Sol. Cells* **2018**, *179*, 334–338. [CrossRef]
204. Wong, B.W.A.; Gamel, M.M.A.; Lee, H.J.; Rashid, W.E.; Yao, L.K.; Jern, K.P. Simulation and Optimization of Emitter Thickness for Indium Arsenide-Based Thermophotovoltaic Cell. In Proceedings of the 2019 IEEE Regional Symposium on Micro and Nanoelectronics, RSM 2019, Pahang, Malaysia, 21–23 August 2019; pp. 133–136.
205. Zhang, X.L.; Huang, A.B.; Tian, C.Y.; Wang, Y.; Lou, Y.Y. Thermophotovoltaic Generation of Electricity with InAs0.91Sb0.09 Device. *IEEE Trans. Electron Devices* **2018**, *65*, 4429–4433. [CrossRef]
206. Vaillon, R.; Pérez, J.-P.; Lucchesi, C.; Cakiroglu, D.; Chapuis, P.-O.; Taliercio, T.; Tournié, E. Micron-sized liquid nitrogen-cooled indium antimonide photovoltaic cell for near-field thermophotovoltaics. *Opt. Express* **2019**, *27*, A11–A24. [CrossRef]
207. Cakiroglu, D.; Perez, J.-P.; Evirgen, A.; Lucchesi, C.; Chapuis, P.-O.; Taliercio, T.; Tournié, E.; Vaillon, R. Indium antimonide photovoltaic cells for near-field thermophotovoltaics. *Sol. Energy Mater. Sol. Cells* **2019**, *203*, 110190. [CrossRef]
208. Xuan, Y.; Chen, X.; Han, Y. Design and analysis of solar thermophotovoltaic systems. *Renew. Energy* **2011**, *36*, 374–387. [CrossRef]
209. Zhou, Z.; Sakr, E.; Sun, Y.; Bermel, P. Solar thermophotovoltaics: Reshaping the solar spectrum. *Nanophotonics* **2016**, *5*, 1–21. [CrossRef]
210. Cmih, C.M.I.H.; Norton, B.; Duffy, A.; Oubaha, M. Hybrid Solar Thermophotovoltaic-Biomass/Gas Power Generation System with a Spectrally Matched Emitter for Lower Operating Temperatures. In Proceedings of the 12th Conference on Sustainable Development of Energy, Water and Environment Systems, Dubrovnik, Croatia, 4–8 October 2017; p. 0563.

211. Davis, G. Hybrid Thermophotovoltaic Power Systems. California energy commission consultant report, 2002 US; P500-02-048F. Available online: https://www.scribd.com/document/138324024/Hybrid-Thermophotovoltaic-Power (accessed on 17 August 2021).
212. Bitnar, B.; Durisch, W.; Holzner, R. Thermophotovoltaics on the move to applications. *Appl. Energy* **2013**, *105*, 430–438. [CrossRef]
213. Chan, W.R.; Stelmakh, V.; Waits, C.M.; Soljacic, M.; Joannopoulos, J.D.; Celanovic, I. Photonic Crystal Enabled Thermophotovoltaics for a Portable Microgenerator. *J. Phys. Conf. Ser.* **2015**, *660*, 012069. [CrossRef]
214. Chan, W.R.; Stelmakh, V.; Karnani, S.; Waits, C.M.; Soljacic, M.; Joannopoulos, J.D.; Celanovic, I. Towards a portable mesoscale thermophotovoltaic generator. *J. Phys. Conf. Ser.* **2018**, *1052*, 012041. [CrossRef]
215. Fraas, L.M.; Avery, J.E.; Daniels, W.E.; Huang, H.X.; Malfa, E.; Venturino, M.; Testi, G.; Mascalzi, G.; Wuenning, J.G. TPV Tube Generators for Apartment Building and Industrial Furnace Applications. *AIP Conf. Proc.* **2003**, *653*, 38–48.
216. Qiu, K.; Hayden, A.C.S. Implementation of a TPV integrated boiler for micro-CHP in residential buildings. *Appl. Energy* **2014**, *134*, 143–149. [CrossRef]
217. Bianchi, M.; Ferrari, C.; Melino, F.; Peretto, A. Feasibility study of a Thermo-Photo-Voltaic system for CHP application in residential buildings. *Appl. Energy* **2012**, *97*, 704–713. [CrossRef]
218. Kilner, J.; Skinner, S.; Irvine, S.; Edwards, P. *Functional Materials for Sustainable Energy Applications*; Woodhead Publishing Limited: Soston, UK, 2012.
219. De Pascale, A.; Ferrari, C.; Melino, F.; Morini, M.; Pinelli, M. Integration between a thermophotovoltaic generator and an Organic Rankine Cycle. *Appl. Energy* **2012**, *97*, 695–703. [CrossRef]
220. Schock, A.; Kumar, V. Radioisotope thermophotovoltaic system design and its application to an illustrative space mission. *AIP Conf. Proc.* **1995**, *321*, 139–152.
221. Wilt, D.; Chubb, D.; Wolford, D.; Magari, P.; Crowley, C. Thermophotovoltaics for Space Power Applications. *AIP Conf. Proc.* **2007**, *890*, 335–345.
222. Teofilo, V.L.; Choong, P.; Chang, J.; Tseng, Y.-L.; Ermer, S. Thermophotovoltaic Energy Conversion for Space. *J. Phys. Chem. C* **2008**, *112*, 7841–7845. [CrossRef]
223. Wang, X.; Chan, W.; Stelmakh, V.; Celanovic, I.; Fisher, P. Toward high performance radioisotope thermophotovoltaic systems using spectral control. *Nucl. Instrum. Methods Phys. Res. Sect. A Accel. Spectrometers Detect. Assoc. Equip.* **2016**, *838*, 28–32. [CrossRef]
224. Li, Q.; Shen, K.; Yang, R.; Zhao, Y.; Lu, S.; Wang, R.; Dong, J.; Wang, D. Comparative study of GaAs and CdTe solar cell performance under low-intensity light irradiance. *Sol. Energy* **2017**, *157*, 216–226. [CrossRef]
225. Wang, X.; Liang, R.; Fisher, P.; Chan, W.; Xu, J. Radioisotope Thermophotovoltaic Generator Design Methods and Performance Estimates for Space Missions. *J. Propuls. Power* **2020**, *36*, 593–603. [CrossRef]
226. Wang, X.; Chan, W.; Stelmakh, V.; Fisher, P. Radioisotope thermophotovoltaic generator design and performance estimates for terrestrial applications. In Proceedings of the International Conference on Nuclear Engineering, Proceedings, ICONE, Shanghai, China, 2–6 July 2017; Volume 3, pp. 1–9.
227. Strauch, J.E.; Klein, A.; Charles, P.; Murray, C.; Du, M. General Atomics Radioisotope Fueled Thermophotovoltaic Power Systems for Space Applications. In Proceedings of the 13th International Energy Conversion Engineering Conference, Orlando, FL, USA, 27–29 July 2015; pp. 366–374.
228. Bauer, T.; Forbes, I.; Pearsall, N. The potential of thermophotovoltaic heat recovery for the UK industry. *Int. J. Ambient. Energy* **2004**, *25*, 19–25. [CrossRef]
229. Yugami, H. An overview of TPV research activities in Japan. In Proceedings of the AIP Conference Proceedings 738; TPV6: Sixth World Conference on Thermophotovoltaic Generation of Electricity, Freiburg, Germany, 7 December 2004; Volume 738, pp. 15–23.
230. Utlu, Z.; Parali, U. Investigation of the potential of thermophotovoltaic heat recovery for the Turkish industrial sector. *Energy Convers. Manag.* **2013**, *74*, 308–322. [CrossRef]
231. Bauer, T.; Forbes, I.; Penlington, R.; Pearsall, N. The Potential of Thermophotovoltaic Heat Recovery for the Glass Industry. *AIP Conf. Proc.* **2003**, *653*, 101–110.
232. Datas, A.; Ramos, A.; Marti, A.; del Cañizo, C.; Luque, A. Ultra high temperature latent heat energy storage and thermophotovoltaic energy conversion. *Energy* **2016**, *107*, 542–549. [CrossRef]
233. Seyf, H.R.; Henry, A. Thermophotovoltaics: A potential pathway to high efficiency concentrated solar power. *Energy Environ. Sci.* **2016**, *9*, 2654–2665. [CrossRef]
234. Amy, C.; Seyf, H.R.; Steiner, M.A.; Friedman, D.J.; Henry, A. Thermal energy grid storage using multi-junction photovoltaics. *Energy Environ. Sci.* **2019**, *12*, 334–343. [CrossRef]
235. Martín, D.; Algora, C. Temperature-dependent GaSb material parameters for reliable thermophotovoltaic cell modelling. *Semicond. Sci. Technol.* **2004**, *19*, 1040–1052. [CrossRef]
236. Pollak, F.H. Temperature dependence of the energy and broadening parameter of the fundamental band gap using infrared photoreflectance. *Phys. Rev. B* **2000**, *62*, 600–604.
237. Ogbonnaya, C.; Abeykoon, C.; Nasser, A.; Turan, A. Radiation-Thermodynamic Modelling and Simulating the Core of a Thermophotovoltaic System. *Energies* **2020**, *13*, 6157. [CrossRef]
238. Fraas, L.M. *Thermophotovoltaics Using Infrared Sensitive Cells in Low-Cost Solar Electric Power*; Springer International Publishing: Berlin/Heidelberg, Germany, 2014.

239. Nishioka, K.; Ota, Y.; Tamura, K.; Araki, K. Heat reduction of concentrator photovoltaic module using high radiation coating. *Surf. Coatings Technol.* **2013**, *215*, 472–475. [CrossRef]
240. Potter, W.R. Radiative cooling for thermophotovoltaic systems. *Proc. SPIE* **2016**, *997*, 997308.
241. Karthikeyan, V.; Prasannaa, P.; Sathishkumar, N.; Emsaeng, K.; Sukchai, S.; Sirisamphanwong, C. Selection and preparation of suitable composite phase change material for PV module cooling. *Int. J. Emerg. Technol.* **2019**, *10*, 385–394.
242. Gamel, M.; Jern, K.P.; Rashid, E.; Jing, L.H.; Yao, L.K.; Wong, B. Effect of Front-Surface-Field and Back-Surface-Field on the Performance of GaAs Based-Photovoltaic Cell. In Proceedings of the 2019 IEEE International Conference on Sensors and Nanotechnology, Penang, Malaysia, 24–25 July 2019; pp. 1–4.
243. Van Der Heide, J.; Posthuma, N.; Flamand, G.; Geens, W.; Poortmans, J. Cost-efficient thermophotovoltaic cells based on germanium substrates. *Sol. Energy Mater. Sol. Cells* **2009**, *93*, 1810–1816. [CrossRef]
244. Kaneko, T.; Kondo, M. High Open-Circuit Voltage and Its Low Temperature Coefficient in Crystalline Germanium Solar Cells Using a Heterojunction Structure with a Hydrogenated Amorphous Silicon Thin Layer. *Jpn. J. Appl. Phys.* **2011**, *50*, 23–26. [CrossRef]
245. Nakano, S.; Takeuchi, Y.; Kaneko, T.; Kondo, M. Influence of surface treatments on crystalline germanium heterojunction solar cell characteristics. *J. Non. Cryst. Solids* **2012**, *358*, 2249–2252. [CrossRef]
246. Hitchcock, C.; Gutmann, R.; Borrego, J.; Ehsani, H. GaInSb and GaInAsSb Thermophotovoltaic Device Fabrication and Characterization. In Proceedings of the Thermophotovoltaic Generation Electricity Third NREL Conference, Colorado Springs, CO, USA, May 1997; Volume 89.
247. Lim, M.; Lee, S.S.; Lee, B.J. Effects of multilayered graphene on the performance of near-field thermophotovoltaic system at longer vacuum gap distances. *J. Quant. Spectrosc. Radiat. Transf.* **2017**, *197*, 84–94. [CrossRef]
248. Lim, M.; Song, J.; Kim, J.; Lee, S.S.; Lee, I.; Lee, B.J. Optimization of a near-field thermophotovoltaic system operating at low temperature and large vacuum gap. *J. Quant. Spectrosc. Radiat. Transf.* **2018**, *210*, 35–43. [CrossRef]
249. Zhao, B.; Santhanam, P.; Chen, K.; Buddhiraju, S.; Fan, S. Near-Field Thermophotonic Systems for Low-Grade Waste-Heat Recovery. *Nano Lett.* **2018**, *18*, 5224–5230. [CrossRef] [PubMed]
250. Fiorino, A.; Zhu, L.; Thompson, D.; Mittapally, R.; Reddy, P.; Meyhofer, E. Nanogap near-field thermophotovoltaics. *Nat. Nanotechnol.* **2018**, *13*, 806–811. [CrossRef] [PubMed]
251. Datas, A. Hybrid thermionic-photovoltaic converter. *Appl. Phys. Lett.* **2016**, *108*, 143503. [CrossRef]
252. Bellucci, A.; Mastellone, M.; Serpente, V.; Girolami, M.; Kaciulis, S.; Mezzi, A.; Trucchi, D.M.; Antolin, E.; Villa, J.; García-Linares, P.; et al. Photovoltaic Anodes for Enhanced Thermionic Energy Conversion. *ACS Energy Lett.* **2020**, *5*, 1364–1370. [CrossRef]